

# **In-Line Nondestructive Inspection of Mechanical Defects in Pipelines with Shear Horizontal Wave EMAT**

**Contract #:** DTRT57-06-C-10004

Final Report

Presented to:

Mr. Merritt

Department of Transportation  
Office of Pipeline Safety  
793 Countrybriar Lane  
Denver, CO 80129  
(303) 683-3117

Submitted by:



Intelligent Automation, Inc.  
15400 Calhoun Dr, Suite 400  
Rockville, MD 20855

These SBIR data are furnished with SBIR rights under Contract No DTRT57-06-C-10004. For a period of 4 years after acceptance of all items to be delivered under this contract, the Government agrees to use these data for Government purposes only, and they shall not be disclosed outside the Government (including disclosure for procurement purposes) during such period without permission of the Contractor, except that, subject to the foregoing use and disclosure prohibitions, such data may be disclosed for use by support Contractors. After the aforesaid 4-year period the Government has a royalty-free license to use, and to authorize others to use on its behalf, these data for Government purposes, but is relieved of all disclosure prohibitions and assumes no liability for unauthorized use of these data by third parties. This Notice shall be affixed to any reproductions of these data, in whole or in part.

# In-Line Nondestructive Inspection of Mechanical Defects in Pipelines with Shear Horizontal Wave EMAT

Final Report

Performance period November 9, 2005 – May 9, 2006

Submitted by Intelligent Automation, Inc.  
George Zhao, Gang Mei and Hongda Chen

Oak Ridge National Lab  
Venu Varma

1. Summary .....	2
2. Technical Achievements .....	3
2.1 Review of the project objectives.....	3
2.2 Theoretical modeling of SH wave incident into the dents.....	3
2.3 Mechanical fixture design for dynamic data collection.....	7
2.3.1 Mechanical Design.....	7
2.3.2 Dent Creation.....	10
2.3.3 EMAT data collection.....	12
2.4 Data Processing.....	14
2.4.1 Preprocessing for removal of abnormal waveforms.....	14
2.4.2 Initial studies on dent detection.....	17
2.5 Classification of Mechanical Defects in Pipelines.....	20
2.5.1 Support Vector Machine (SVM).....	21
2.5.2 Feature Extraction.....	22
2.5.3 Performance Evaluations.....	32
2.5.4 Concluding Remarks.....	37
3. Future Work.....	37
Acknowledgments.....	39

## 1. Summary

Pipelines used for transporting natural gas and petroleum fluid are aging and may suffer from accidental damage. Historically, mechanical damage is the single largest cause of failures on those pipelines. There are about 160 pipeline companies in the United States, operating over 285,000 miles of pipe. The need is growing for an efficient and reliable inspection system to locate and characterize the weak spots as early as possible to save cost and for public safety. Axial and circumferential field magnetic flux leakage (MFL) in-line inspection (ILI) smart PIG and compression wave ultrasonic transmission devices, currently used for detecting metal loss and other defects like Stress Corrosion Cracks (SCC), have the difficulty of reliably detecting the coincidental metal loss associated with the “cup” type injurious anomaly.

Intelligent Automation, Incorporated (IAI) and Oak Ridge National Lab (ORNL) worked on a novel and integrated approach to inspect mechanical damages in pipes. State-of-the-art Shear Horizontal (SH) wave EMAT sensors are mounted on a rugged mobile fixture that can go inside

the pipe and collect ultrasonic guided wave data while traveling in the pipe. Through a two-dimensional (2-D) and 3D Boundary Element Method (BEM) modeling, the scattering responses of the dents are calculated to provide physical insight of the inspection technology and guidelines for sensor designs. Circumferential SH waves in a through transmission mode were collected. Various defect features such as the signal energy, the power density spectrum, and the *Kullback Leibler* distance (KL-distance)<sup>1</sup> of defect signal to the normal condition were extracted. Pattern classification algorithms such as Principal Component Analysis (PCA)<sup>2</sup> and Discriminant Analysis (DA), as well as support vector machines were used to detect and classify the “Cup” and “Saucer” shaped dents in the pipe specimens. The technique is successful to detect any dents that deform 25% of the pipe wall thickness in a seamless pipe, and the classification rate between “Cup” and “Saucer” shapes at that depth level is nearly 100%.

In the next sections, the technical details of the work performed are presented. The potential Phase 2 activities are also included.

## **2. Technical Achievements**

### **2.1 Review of the project objectives**

After the project started, we arranged a kick-off teleconference with Mr. Merritt of PHMSA. From the meeting and several correspondences afterwards, we were able to finalize task plans. For the phase I project, we will stick to 12” pipe and do all the preliminary proof-of-principle demonstration. Our fixture was designed in a way it can accommodate 8 inch to 12 inch diameter pipes. Also, the data is collected while the EMATs are moving with respect to the defects.

In this project, the following issues were addressed according to the work plan: (1) thorough guided wave modal analysis through a three-dimensional (3-D) Boundary Element Method (BEM) modeling for wave scattering analysis around the circumference of the dents and for defect volumetric feature extraction, (2) Both circumferential and axial ultrasonic SH wave EMAT will be used for collecting data and analysis, (3) Refine the dents detection and classification algorithm such as Principal Component Analysis (PCA) and Discriminant Analysis (DA) for mechanical defect signature extraction and pattern classification, and (4) small dents assessment. The envisioned system will be mounted on a PIG for accurately and reliably detecting the metal loss and other defects in the pipeline infrastructures long before they need remediation.

### **2.2 Theoretical modeling of SH wave incident into the dents**

Consider a sample 3-D problem as shown in Fig. 1, where an infinitely large flat plate has a 3-D arbitrary shaped defect. A time-harmonic guided plane wave (either Lamb wave or SH wave) is incident in the positive x direction. Due to the acoustic impedance mismatch at the defect, the guide wave mode incident into the defects results in scattered waves of all orders of the propagating as well as non-propagating modes (both Lamb wave and SH waves) at the vicinity of the defect. The evanescent modes die out quickly within several wavelengths, thus only propagating modes survive and carry out energy flux at the far-field from the defect. At different

---

<sup>1</sup> Cover, T. M. and Thomas, J. A. *Elements of Information Theory*. New York: Wiley, 1991.

<sup>2</sup> S. Haykin, *Neural Networks*, Prentice-Hall, 1990.

directions, the wave displacement and stress fields are different in general and form an angular pattern. For different defects, this pattern will also be different, which could be used for defect shape and sizing analysis.

In order to calculate the scattered wave field, the hybrid BEM normal mode expansion technique that was successfully applied to the 2-D defect characterization problem<sup>3</sup> was extended to the 3-D cases. In specific, a virtual cylinder enclosing the region with defects was defined for BEM meshing. The radius of the disc region is larger than the largest wavelength of all possible propagating guided wave modes in the plate. A cylindrical coordinate system was established at the center of the disc region, with the  $z=0$  plane coinciding with the mid-plane of the plate. Outside the defined defect region, the total displacement and traction field are the superposition of all the incident and scattered propagating wave modes. Within the defect region, the 3-D elastodynamic BEM was used to calculate the wave field. Upon boundary conditions being specified at the virtual cylindrical boundary, the BEM calculates and outputs the displacement and traction value for each boundary element, from which the scattered wave field is determined and so as each wave mode.

In this study, boundary element modeling (BEM) is set up for calculating the scattering profile of SH wave impinging onto the dent defects. A three dimensional model is setup with a plate having a 50% through wall flat bottom hole. This is just for simplicity and verification purpose. The diagram of the model is shown in Fig. 1. The usage of plate specimen to approximate a 12” standard pipe has been proved valid<sup>4</sup>. Around 1000 elements are used to mesh the boundary of the specimen with the dent defect. Fig. 2 shows the mesh generated by IDEALS 7.0 near the dent.

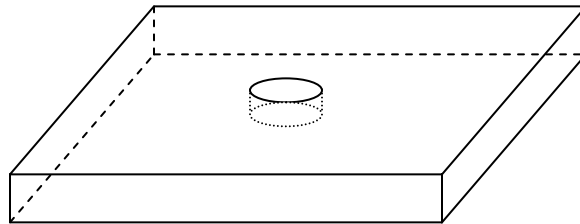


Fig. 1 Diagram of a 3-D dent model on a plate. The plate is 10mm thick which is about the thickness of a 12” pipe wall. The dent is 10mm in radius and 50% of wall thickness in depth.

---

<sup>3</sup> X. Zhao et al, “Guided Shear Horizontal (SH) Wave Electromagnetic Acoustic Transducer (EMAT) for In-line Nondestructive Inspection of Pipelines” Final report to DOT contract number DTRS57-04-C-10053, 2005.

<sup>4</sup> X. Zhao, J. L. Rose, “Guided circumferential shear horizontal waves in an isotropic hollow cylinder,” *J. Acoust. Soc. Am.*, Vol. 115, 1912-1916, 2004.

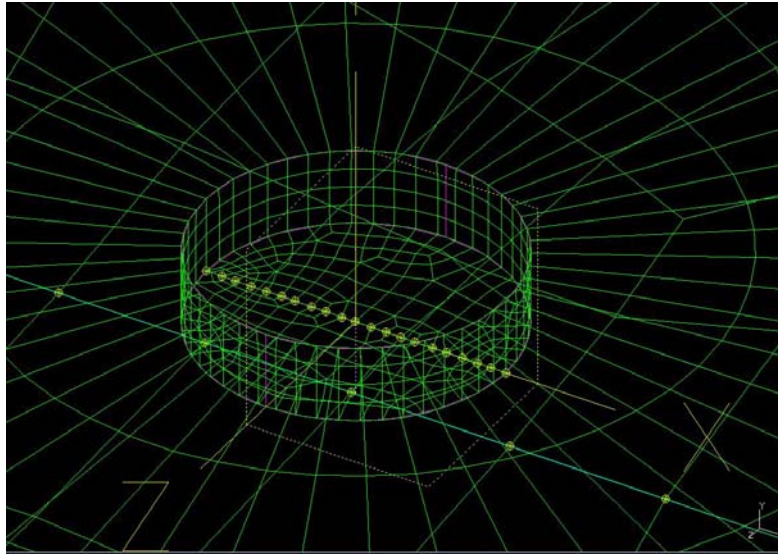
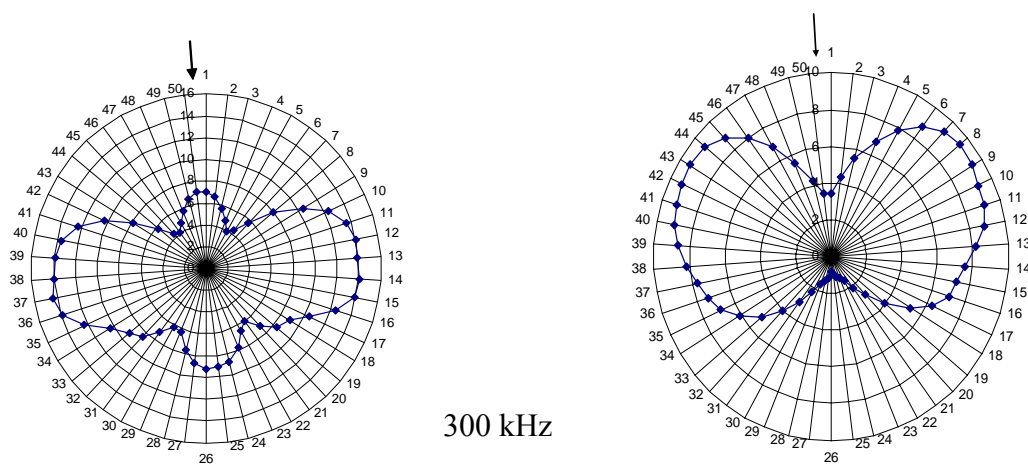
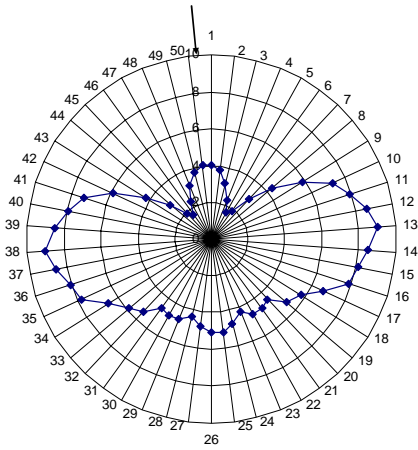


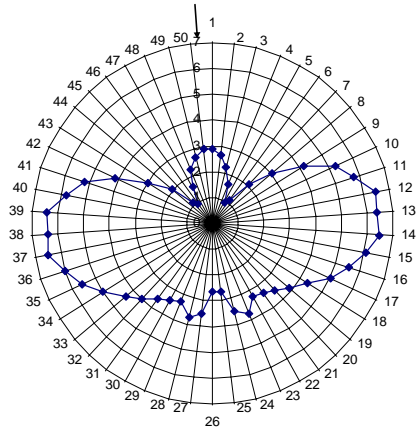
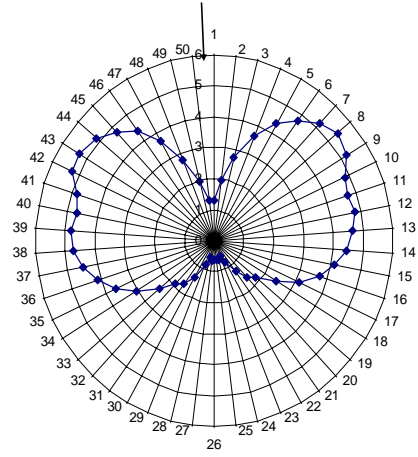
Fig. 2 mesh generated by IDEALS at the dent region.

Fig. 3 shows the calculation results of the SH wave scattering from the dent for different frequencies. A plane SH wave at 30 to 120 kHz is incident into the dent. Upon interaction with the dent, the wave scattered in all the directions. The wave amplitude of the scattered (a) SH wave and (b) the mode converted Lamb wave mode are plotted versus the angular directions. It can be seen that the wave scattering pattern changes with respect to frequencies. The incident direction (marked as an arrow in the plot) shows the direction of the plane SH wave. The wave displacement or particle velocity profiles are plotted with respect to the angular directions. It is also seen that the wave scattering is symmetric with respect to the incident direction (marked as an arrow in the plot). This profile will be different for different defects, which could be useful for defect classification purpose. Also note that even though SH wave was incident, the mode conversion occurs at the dent, thus Lamb wave generated. It could also be useful if we can detect these mode-converted Lamb waves as an additional feature by a Lamb wave EMAT. The different response at different frequencies shows a hint for better sensor or working condition selection, which is important for better defect detection and classification.

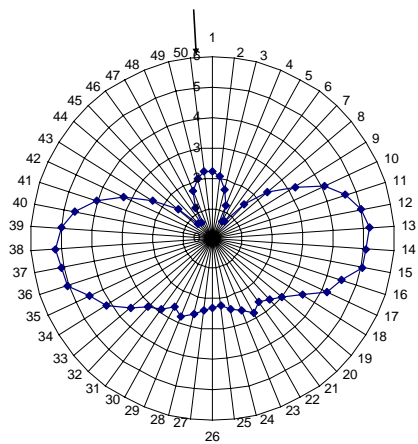
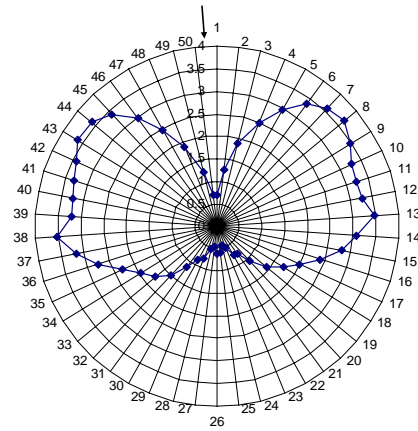




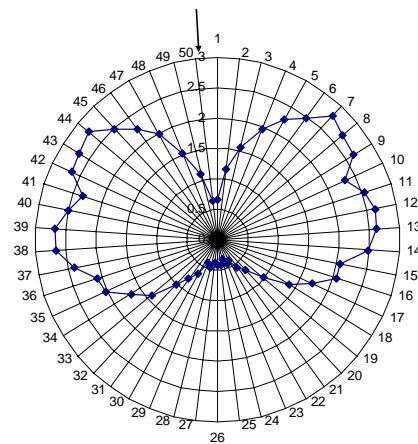
500 kHz



700 kHz



900 kHz



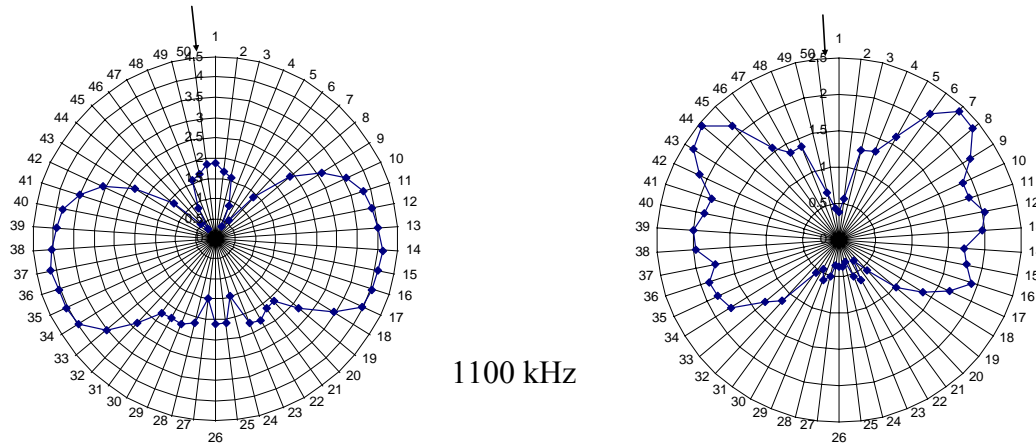


Fig. 3 Scattered wave amplitude (a) SH wave, and (b) mode converted Lamb wave, when a plane SH wave is incident into a 50% through wall dent at different frequencies.

## 2.3 Mechanical fixture design for dynamic data collection

### 2.3.1 Mechanical Design

During the proof-of-principle design stage, EMATs were positioned across the defect to collect data. The EMATs were stationary while the data was being collected. To obtain multiple data points across the same defect, the EMATs were manually positioned across the defect to different relative positions between the sensor and defect. The data collected was sufficient to prove the ability of the EMAT system to detect mechanical dents.

However, during an actual inspection of a pipe, the EMAT probe will be mounted on a moving platform. During the automated acquisition of data, the sensors need to traverse the pipe and collect data without operator interference. The data need to be collected while the EMATs are moving with respect to the defects. To accomplish this a moving platform was designed for carrying the EMATs (see Fig. 4).

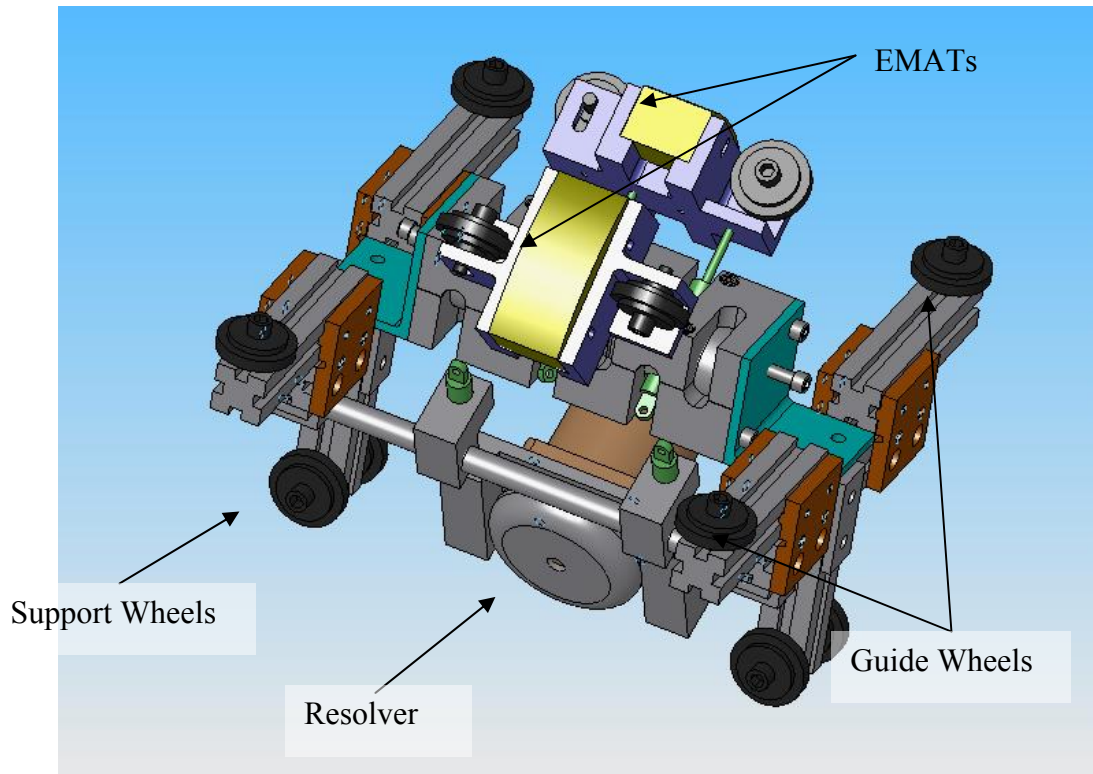


Fig.4. EMAT platform for acquiring dynamic data

The mechanical design of the platform accommodates pipes from 8” to 12” diameter. The main body of the platform consists of an 80/20 frame with provisions for attaching the sensors. Multiple wheels, both fixed and spring loaded support the frame and positions the sensor across the center of the pipe as it traverses.

The EMATs needs to be very close to the pipe wall to obtain very good signal. The signal exponentially decays with larger liftoff from the pipe wall. Hence the sensors are mounted on gas springs that maintain the gap between the pipe wall and sensor surface. Two pairs of wheels maintain the actual lift off between the EMAT and the pipe wall. The wheels are mounted on slots and by adjusting them the actual lift off can be controlled. The wheels allow the sensor to travel along the pipe while maintaining the gap. The support and the guide wheels allow the platform to translate axially along the pipe while maintaining the orientation of the EMATs with respect to the defects. Figure 5 shows the schematic of the circumferential EMAT inside the pipe.

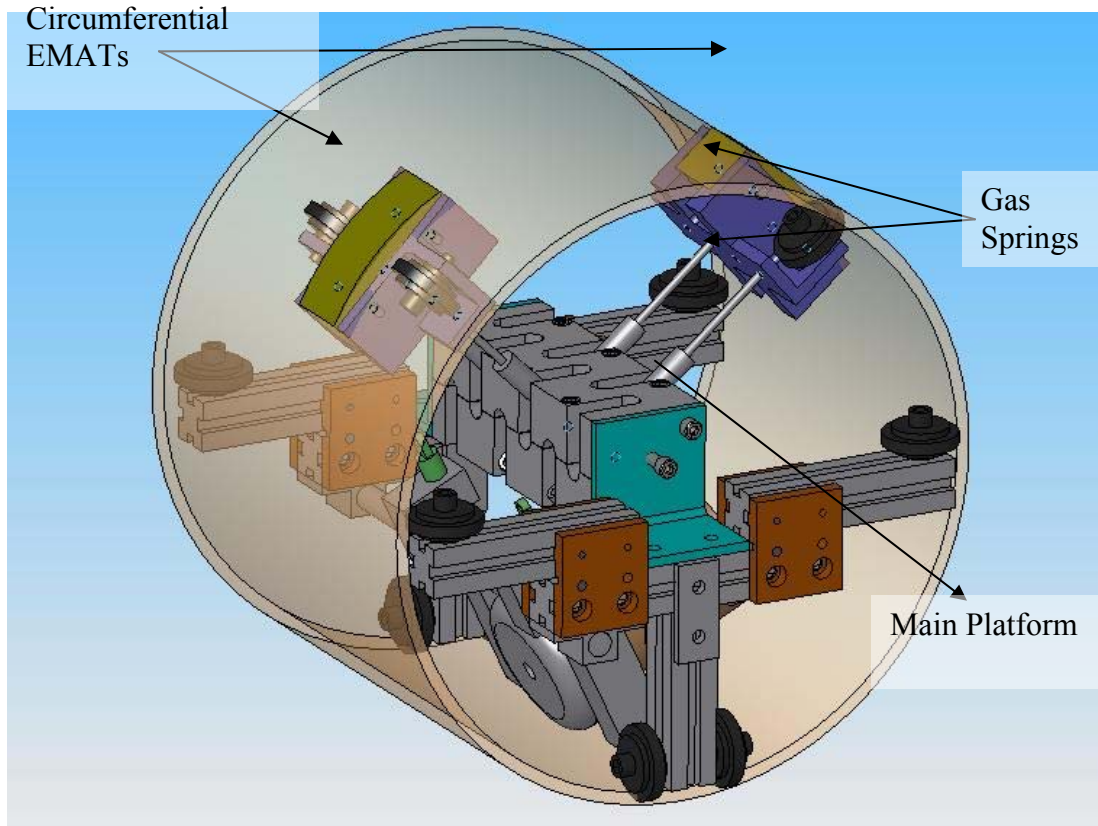


Fig. 5 EMAT platform inside a pipe

To correlate the signal with the position of the sensor inside the pipe, a rotary position sensor (Vishay smart position sensor) with a 3" wheel mounted on it is used. The position sensor with conductive plastic technology is able to provide 360° angular position with 0.5° resolution. As the EMAT is pulled through the pipe, the wheel turns and by counting the number of rotations and the angular position, location of the EMAT is calculated. Every time a signal is obtained from the EMAT, rotary position is also obtained from the position sensor.

The platform was designed to accommodate both an axial and circumferential configuration of the EMATs. Gas springs on which the EMATs are mounted can be rotated and locked in position at the desired orientation. This allows for changing the angular distance between the EMATs in the circumferential configuration. For thinner pipe wall, the distance between EMATs can be larger since the signal is more powerful while using the same tone burst card settings. For the current set-up of 0.375" pipe wall thickness, the distance between the EMATs is fixed at 12 inches end-to-end. In the axial configuration, the EMAT distance is fixed at 11 inches end-to-end.

Figure 6 show the EMAT platform build at ORNL. To obtain dynamic EMAT measurements, the platform was pulled using a winch. An eyebolt was attached to the 80/20 platform for attaching the winch. A constant speed was maintained during the pull. The speed of pull was adjusted by varying the voltage to the winch.

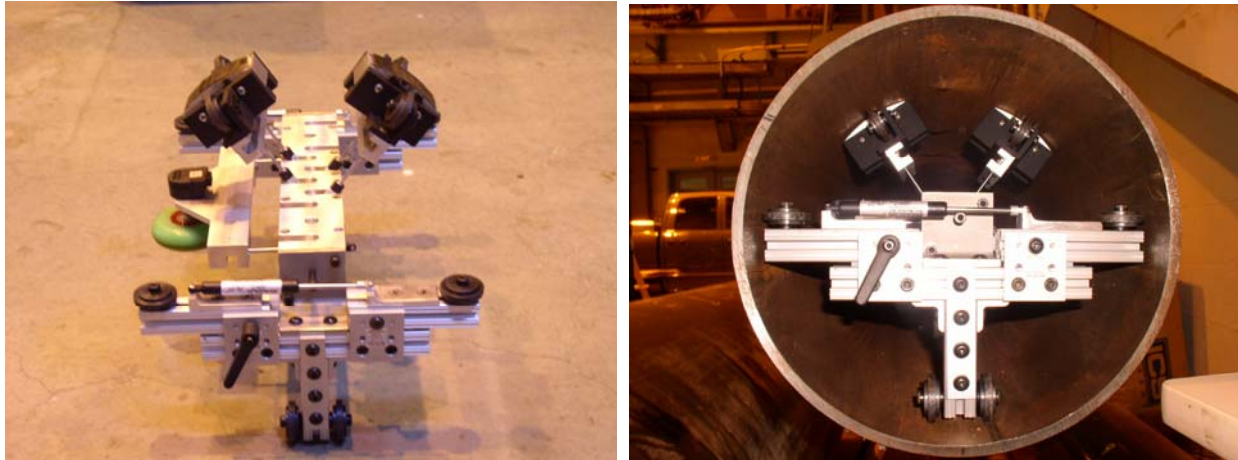


Fig. 6 EMAT platform fabricated at ORNL

### 2.3.2 Dent Creation

Dents on the pipes were created using a hydraulic press. In simulating dents, the dents were classified into cups and saucers. The differentiation of a cup and a saucer is based on the severity of the slope of the defect.

Chrome finish steel balls of 5-inch, 3.75-inch, 1-inch and 0.75-inch diameter were used for the creation of dents. The pipe was placed on the hydraulic press with support braces under it. A fixture attached to the ram on the hydraulic press secured the steel balls. By controlling the amount of displacement of the ram, the dents of different depth were created. The larger diameter balls were used to create saucer while the smaller ones produced the cups.

Figure 7 gives an example of the cup and saucer created on the 12-inch diameter pipe. Two pipes with different dent sizes were created for these experiments. One pipe had a single row of dents while the other has three rows of dents each radially spaced 120° apart.

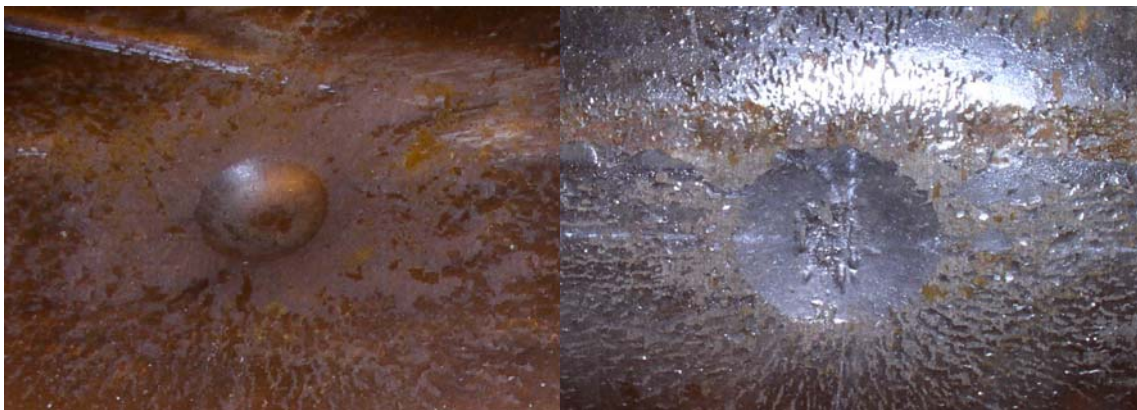


Fig. 7 Cup and saucer on a 12-inch pipe

Fig. 8 illustrates the pipe specimens and the dents. The lengths of the pipes to be inspected are 85.0625 inches. There are 10 dents in one line on pipe #1 and 16 dents in three lines on pipe #2. The positions and types of these dents are shown in the table 1 and 2. The details of these dents are shown in the following table and picture.

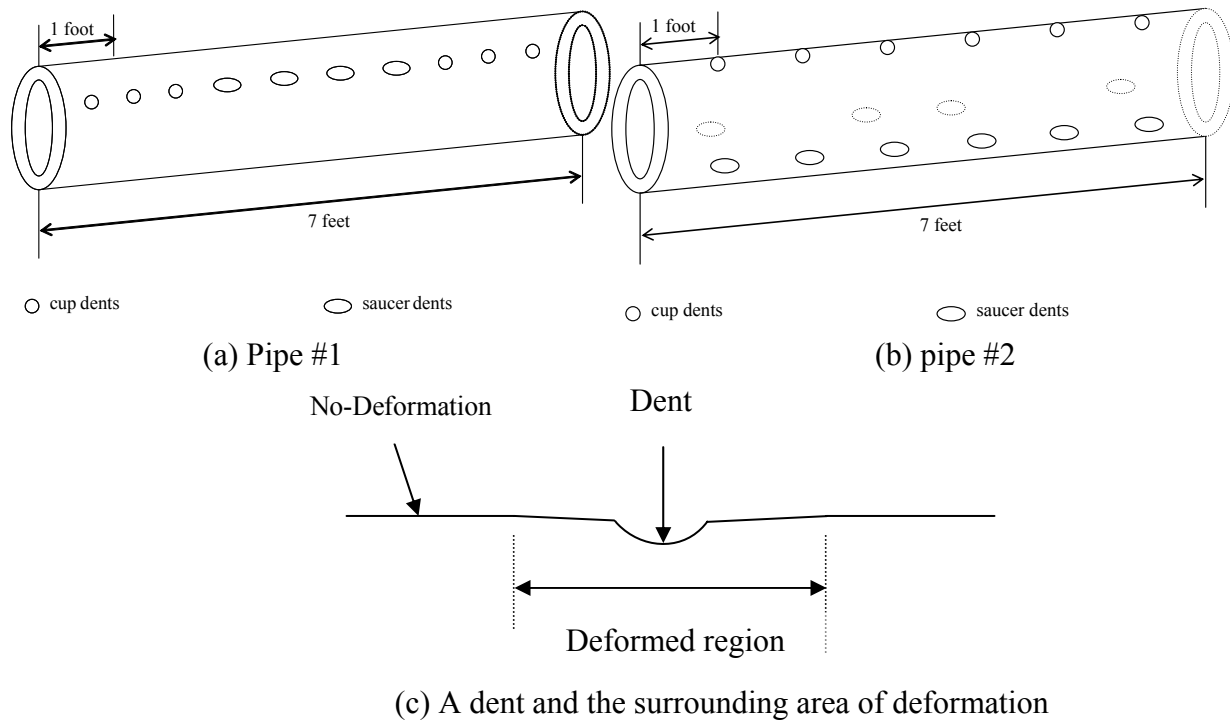


Fig. 8 illustration of the pipe specimens and the formation of deformation due to dents

**Table 1 Dents description on pipe #1**

Dent number, type and position (inch)	Diameter (inch)		Depth (inch)	Area of deformation	Ball Diameter (inch)
	Axial	Circumferential			
1 Cup (6.75)	0.59	0.59	0.238	1.8 x 1.3	1
2 Cup (14.9375)	0.65	0.65	0.345	3.5 x 2.2	
3 Cup (23.125)	0.63	0.63	0.318	2.5 x 1.6	
4 Saucer (31.3758)	1.185	1.02	0.305	3.2 x 2.2	3.75
5 Saucer (39.5625)	1.5	1.294	0.499	5 x 3.2	
6 Saucer (47.3125)	1.34	1.14	0.283	3 x 2	5
7 Saucer (55.25)	1.79	1.4	0.358	4.4 x 2.8	
8 Cup (63.375)	0.515	0.515	0.220	1.50x 1.3	0.75
9 Cup (71.375)	0.5	0.5	0.198	1.5 x 1.3	
10 Cup (79.4375)	0.546	0.54	0.249	1.8 x 1.5	

**Table 2 Dents description on pipe #2**

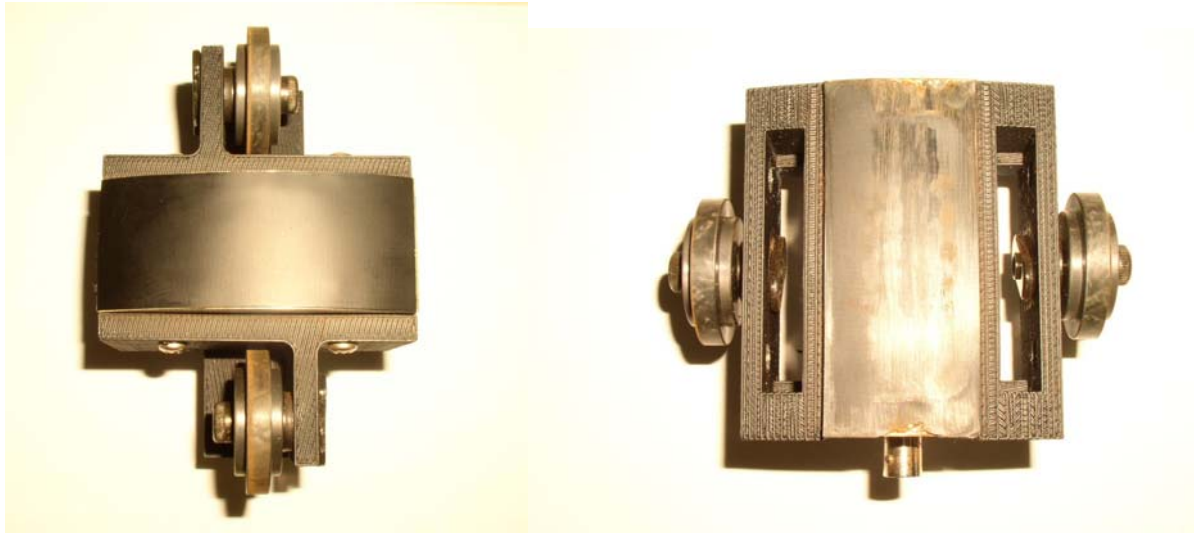
Dent number, type and position (inch)	Diameter (inch)		Depth (inch)	Area of deformation	Ball Diameter (inch)
	Axial	Circumferential			
1 Cup (11.53)	0.395	0.378	0.085	0.63 x 0.55	0.75
2 Cup (23.75)	0.5	0.488	0.218	1.4 x 0.75	
3 Cup (35.81.25)	0.444	0.435	0.124	0.95 x 0.75	
4 Cup (48)	0.415	0.415	0.065	0.625 x 0.625	1
5 Cup (60.3125)	0.545	0.534	0.20	1.35 x 1.2	
6 Cup (72.375)	0.386	0.375	0.062	0.55 x 0.51	
7 Saucer (12.5625)	0.72	0.65	0.033	1.25 x 0.875	3.75
8 Saucer (24.75)	1.35	0.995	0.118	3 x 3	
9 Saucer (37.125)	0.595	0.526	0.04	1.25 x 0.95	
10 Saucer (48.9375)	1.46	0.855	0.134	2.4 x 1.56	5
11 Saucer (61)	1.46	0.894	0.121	1.6 x 1.3	
12 Saucer (72.8125)	0.73	0.715	0.094	1.1 x 1.1	
13 Saucer (12.0)	0.615	0.547	0.070	0.95 x 0.65	3.75
14 Saucer (36.75)	0.875	0.775	0.179	1.75 x 1.3	3.75
15 Saucer (48.6875)	0.886	0.75	0.123	1.5 x 1	5
16 Saucer (72.53)	0.745	0.62	0.076	1.1 x 0.85	5

**2.3.3 EMAT data collection**

To collect the data, the platform was pulled through the dented pipe using a winch. Figure 9 shows the circumferential and axial EMAT modules used for these testing. The EMATs in the circumferential configuration were positioned so that the dents were at the midpoint between the receiver and transmitter EMATs. Since the eyebolt was located at the center of the platform and the pull direction was parallel to the axis of the pipe, it did not rotate the platform as it moved through the pipe. For each line (row of dents) five data collection runs were performed. With multiple runs, the consistency of the data could be ascertained.

For the axial configuration, the EMATs were aligned axially along the pipe coinciding with the dent line. Although data was obtained for one line, while taking data on the second line, the gas springs bend. The EMAT got stuck in a large saucer dent and the winch pulling on it bent the gas springs. The gas springs had the ability to compress and advance through the dent, but the design prevented the compression of the springs.

This failure could be fixed by positioning the roller along the axis of travel. This was not possible in the current design due to the location of the co-axial cable connection of the EMAT (see Figure 9). If the roller traveled the same path as the EMATs, it would compress the gas springs sufficiently for the EMATs to pass and not get stuck. Also incorporating a wider wheel would provide better correction margins for large dents.



*a) Circumferential*

*b) Axial*

Fig. 9 Axial and Circumferential EMAT modules

The data collection was taken place on two pipes with the mechanical dents. For the circumferential EMAT data collection on pipe #1, the run started at dent #10 and went towards dent 1. The total length of the platform is 15.625 inches. The location of the EMAT center on the platform from the pull direction is 7.9375 inches. 5 runs have been made for this pipe and the datasets collected are data11, data12, data13, data14 and data15. The following table shows the platform start and end positions for each run. The number is with respect to the pipe edge at each side. Negative means the edge of the platform is extruded from the pipe.

File Name	Begin position (from far end 'dent 10")	End position (dent 1 end)
Data 11	0	0.125"
Data 12	0	-0.125"
Data 13	0	0.0625"
Data 14	0	0.0625"
Data 15	0	0

Similar EMAT data collection was carried out on pipe #2. The following table shows the start and end positions of the platform for each run.

File Name	Begin position (from far end 'dent 10")	End position (dent 1 end)	Explanation
Circumferential data ---- Gain 70 db			
Data 21c	0	-0.25"	Pipe2 dents from 7-12, pull direction from 12 to 7
Data 22c	0	0.1875"	
Data 23c	0	-0.0625"	
Data 24c	0	0.0625"	
Data 25c	0	0.125"	

Data 31c	0	0.0625"	Pipe2 dents from 1-6, pull
Data 32c	0	-0.0625"	(pulled at high speed ) direction from 6 to 1
Data 33c	0	0.0	
Data 34c	0	0.0	
Data 35c	0	0.125	
Data 41c	0	-0.125"	Pipe2 dents from 13-16, pull
Data 42c	0	-0.0625"	direction from 16 to 13
Data 43c	0	0.125"	
Data 44c	0	0.1875"	
Data 45c	0	0.25	

## 2.4 Data Processing

### 2.4.1 Preprocessing for removal of abnormal waveforms

In each of the dataset shown above, there are thousands of waveforms collected when the platform is moving from one end of the pipe to the other. A typical waveform is shown in Fig. 10. However, due to occasional synchronization problems between the data acquisition card and the EMAT sensors and also the potential EMAT circuit problem, there are waveforms that seems abnormal, see Fig. 11. We have developed a preprocessing algorithm to remove those abnormal waveforms from the dataset.

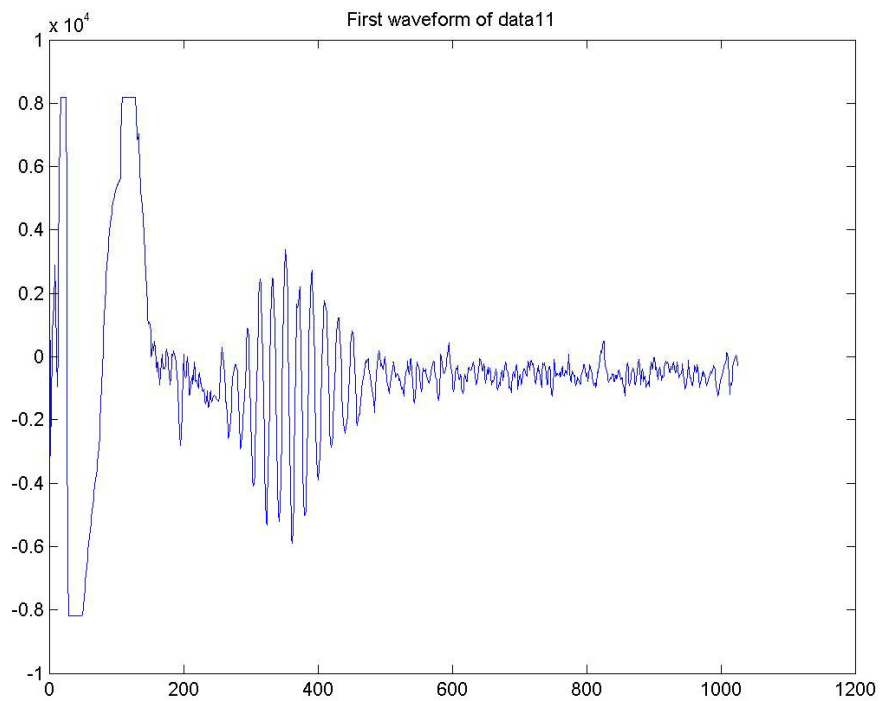


Fig. 10 Typical EMAT waveform

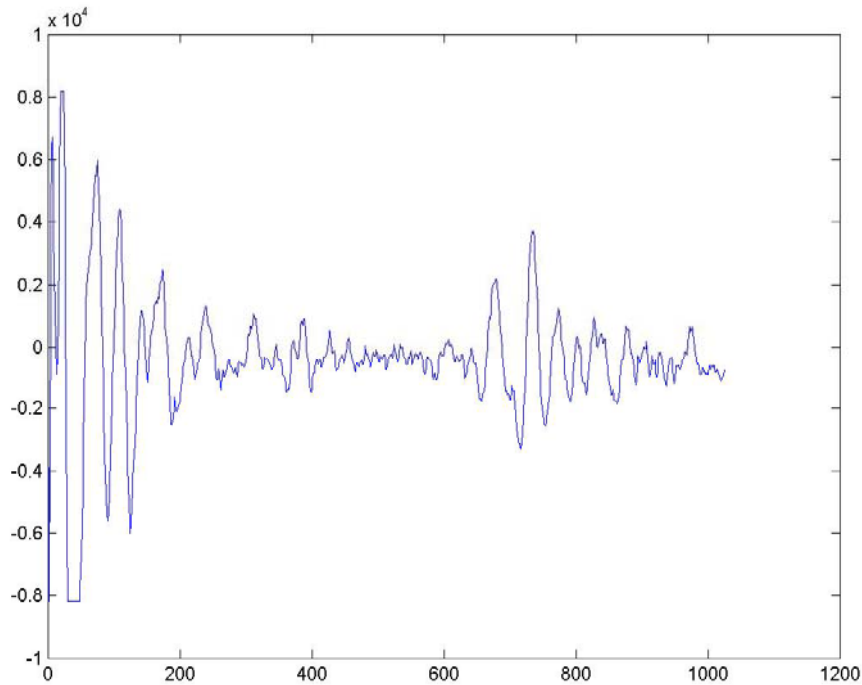


Fig. 11 example abnormal waveforms due to EMAT sensor inconsistency

Here we determine a waveform to be abnormal under one of the following conditions:

- Its correlation and amplitude are both dramatically different than its neighboring waveforms.
- Its main bang doesn't appear in the beginning of the waveform.
- The energy of signal from sampling point of 200 to end doesn't concentrate mainly in the interval from 200 to 600.

Another approach we used to mitigate the abnormal waveform problem is to use only the waveform from index 200 to 600 instead of from index 200 to end. Fig. 12 and 13 show the difference in the signal amplitude plots caused by the abnormal waveform removing. Compare Fig. 13 with Fig. 12, it clearly seen the effect of abnormal waveform removal. This is also important for further processing the data for dent detection and localization.

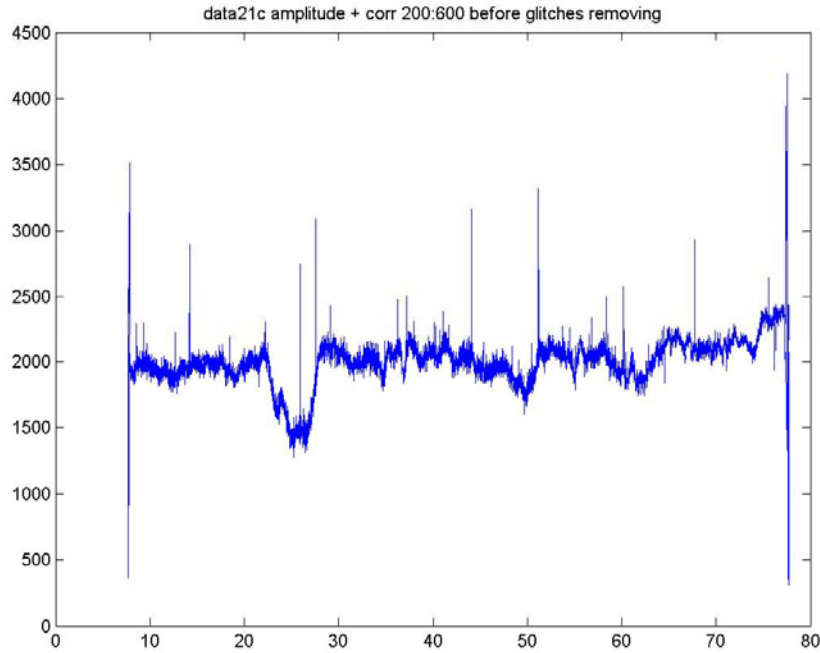


Fig.12 Collected through-transmission EMAT signal amplitude vs. locations in pipe #2 without preprocessing

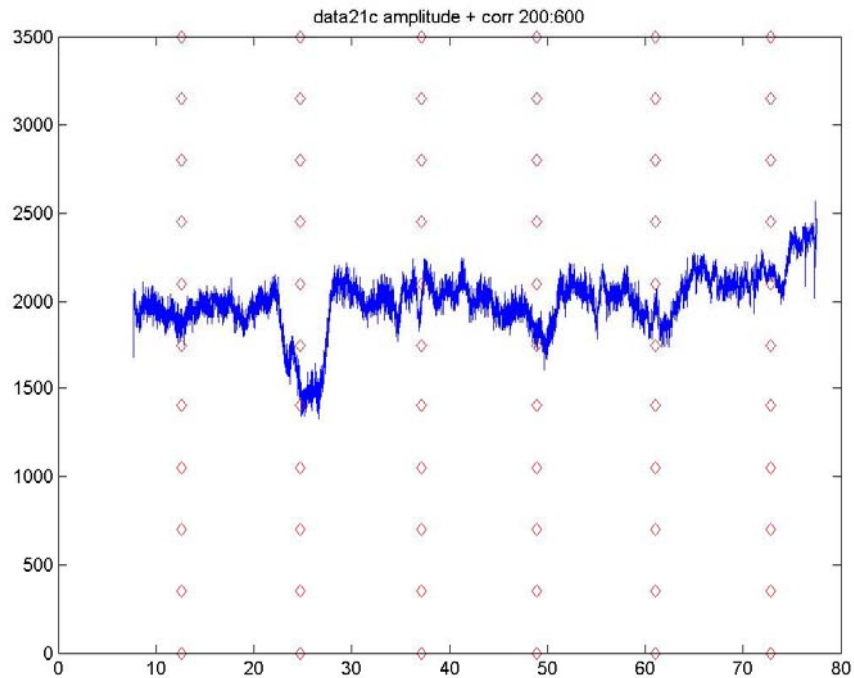


Fig. 13 EMAT signal amplitude plot after removing abnormal waveforms. The red diamonds shows the true dent locations.

## 2.4.2 Initial studies on dent detection

One way to detect the dent is to compare the shape of the waveform at a particular location with a standard template waveform corresponding to the normal condition. Here, we use the starting normal waveforms as the template as shown in Fig. 10, and calculate the correlation coefficient between the collected waveforms and the template waveform. Note that only the useful signal portion which corresponds to the through-transmission signal was truncated for the calculations. The phase shifting between different waveforms was compensated by over-sampling the waveforms and shifting them back until the maximum correlation is reached. The correlation coefficient result for data11 is shown in **Error! Reference source not found.**<sup>14</sup>. The locations of the dents are shown with red diamond columns.

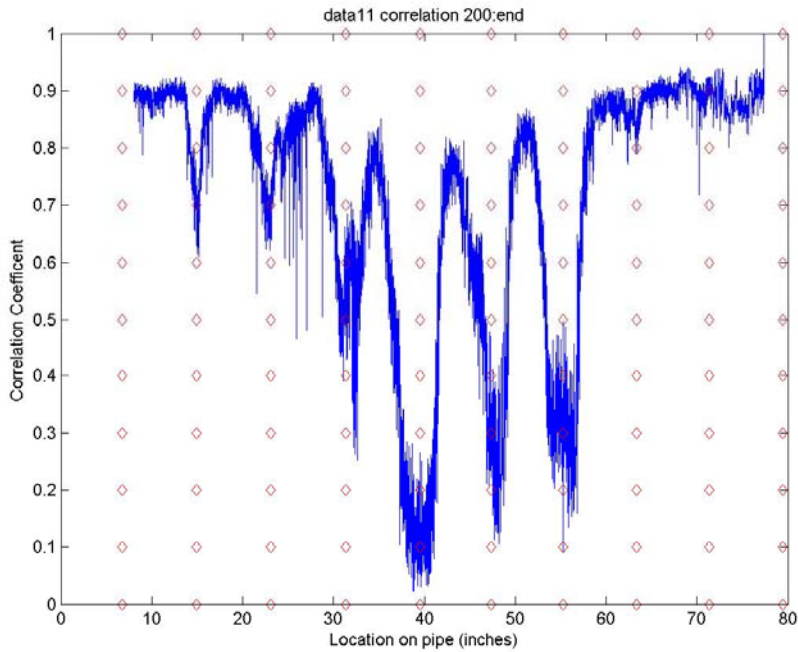


Fig. 14 Correlation coefficients of collected waveform with respect to a normal-condition template when the EMAT goes through the pipe

Another way to detect the dent is to use the amplitude of the collected signal. Again, we only use valid signal portion, which we choose to be the portion started from 200. The amplitude result for data11 is shown in Fig. 15. From Fig. 14 and Fig.15, the following observations can be clearly made.

- Locations of these dents overlap with the bottoms of correlation coefficient curve as well as amplitude curve.
- Bottoms corresponding to the saucers are deeper and more visible than bottoms corresponding to the cups.
- The pipe area between saucers, although has no dents, still has lower correlation coefficient and amplitude than the normal value. It seems that deep dents can cause some spreading effect on neighboring area.

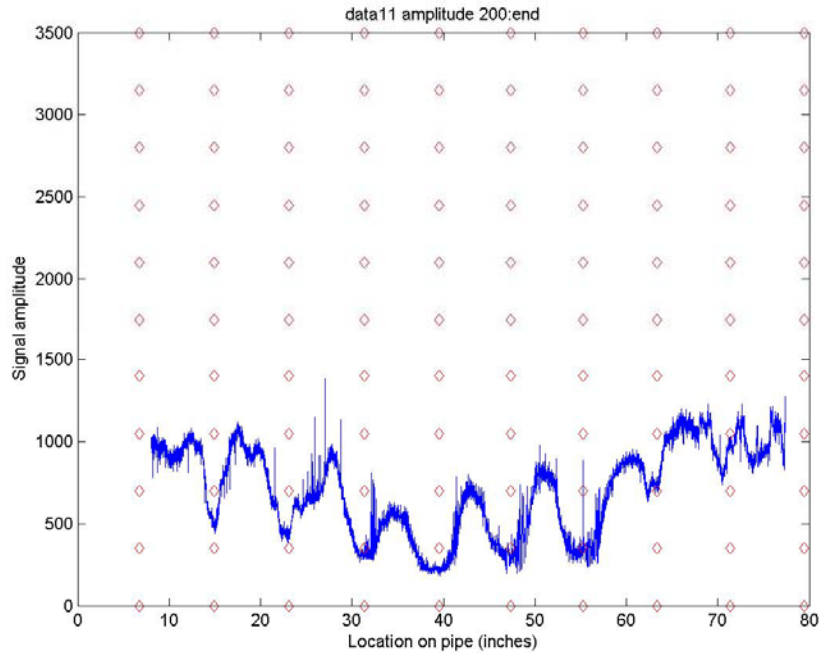


Fig.15 Signal amplitude vs. location on pipe #1

Since the correlation coefficient and amplitude both can be used to detect the dents, to improve the performance, we can add them up after appropriate weighting. The result is shown in **Error! Reference source not found.16** which demonstrates better dent detection capability than only using correlation coefficient or signal amplitude alone.

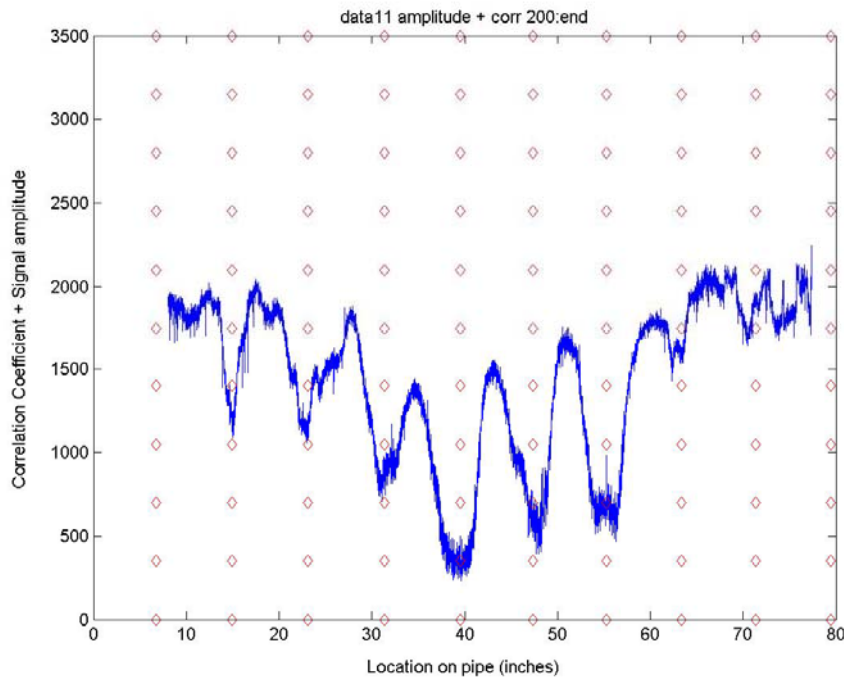


Fig.16 Weighted correlation coefficient value plus amplitude vs. dent location on pipe #1

The results of this algorithm applied on all 5 datasets on pipe #1 for dent locations (in inches):

<i>data11</i>	14.9750	22.9877	31.0676	39.5776	47.9265	55.8355	62.3054	70.4464
<i>data12</i>	15.1846	22.3126	30.8035	39.6489	49.6854	55.1963	62.3599	70.4044
<i>data13</i>	14.9432	22.4887	30.7458	39.4991	47.0139	55.4314	62.4274	71.5027
<i>data14</i>	15.1662	23.0520	31.0616	39.7834	47.2249	55.2507	62.4129	71.4836
<i>data15</i>	15.2893	22.7862	31.8016	40.5033	48.2634	55.1873	63.1101	70.5199

Compare to the measured true locations (inches):

14.9375	23.125	31.3758	39.5625	47.3125	55.25	63.375	71.375
---------	--------	---------	---------	---------	-------	--------	--------

The performance is quite reasonable.

Similar process was also done on the pipe #2. From the weighted summation of the correlation coefficient and amplitude plot as shown in Fig.17 for data 21, we can see the detected dents match with the locations of the deep dents on the pipe whose depths are more than 0.1 inch. There are problems of detecting dents of less than 0.1 inch, as reported in our previous project report<sup>5</sup>.

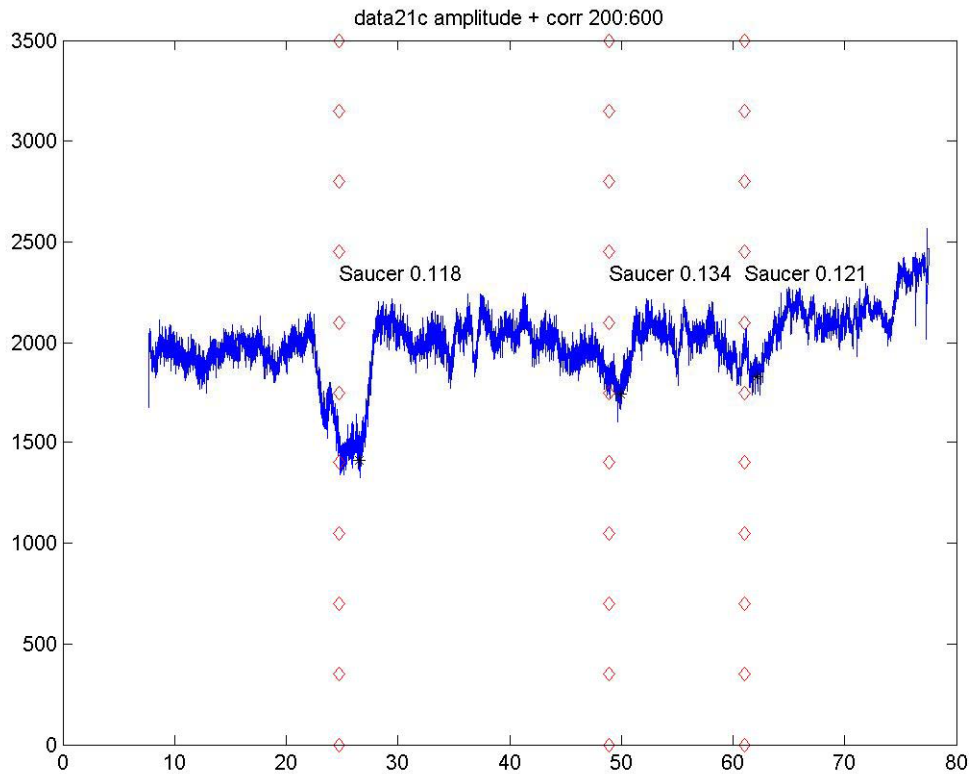


Fig.17: Dent positions using waveform bottoms

<sup>5</sup> X. Zhao et al, "Guided Shear Horizontal (SH) Wave Electromagnetic Acoustic Transducer (EMAT) for In-line Nondestructive Inspection of Pipelines" Final report to DOT contract number DTRS57-04-C-10053, 2005.

The results of this algorithm applied on all datasets are (inches):

*data21c* 26.5191 49.9153 62.1906

*data22c* 25.1066 49.6215 62.1565

*data23c* 26.5264 49.7931 60.1531

*data24c* 26.4916 49.5971 62.1801

*data25c* 25.4260 49.6083 62.2063

*The measured true deep dent locations:* 24.75 48.94 61

*data31c* 24.8653 35.9957 62.1010

*data32c* 24.5951 35.7157 60.6697

*data33c* 24.6923 42.3851 61.8882

*data34c* 24.9613 61.8700

*data35c* 23.7933 35.9268 62.0263

*The measured true deep dent locations:* 23.75 35.81 60.31

*data41c* 37.0854 49.4789

*data42c* 37.3531 49.2558

*data43c* 37.3226 49.7849

*data44c* 37.1723 49.9180

*data45c* 37.2540 49.8545

*The measured true deep dent locations:* 36.75 48.69

## 2.5 Classification of Mechanical Defects in Pipelines

The mechanical dents formed as a result of the damage can usually be divided into two basic groups, namely, “cup” and “saucer” dents. The “saucer” dents are smooth, typically no injurious; however, for “cup” dents that are abrupt, certain range of field conditions including soil type, stress, cathode potential, coating conditions, and temperature, etc. may lead to a catastrophic failure via the coincidental metal loss. It is necessary for an in-line inspection technology to detect, classify, and characterize the mechanical dents on the outer surface of the pipelines.

With the shear horizontal wave EMAT, we have acquired lots of data in different pipeline conditions, including “normal”, “cup” and “saucer” dents for this phase I studies. In order to classify the different types of dents as “cup” and “saucer”, previously, we have used PCA-DA based algorithm which is composed of three major parts: feature extraction by power spectral density (PSD), feature dimension reduction by principle component analysis (PCA), and data classification using discriminant analysis (DA)<sup>6</sup>. However, the classification performance is limited. Referring to Table-3 in [6], the results for the testing data sets regarding the cup/saucer classification are about 66% accuracy there.

---

<sup>6</sup> X. Zhao et al, “In-line nondestructive inspection of mechanical dents in pipelines with guided shear horizontal Electromagnetic Acoustic Transducers,” ASME J. Pres. Ves. Tech. Vol. 127, 304-309, 2005.

To improve classification performance, here, we will use different approaches for cup/saucer classifications. Particularly, we propose to apply the support vector machine (SVM) as the classification component. To apply the SVM, we need feature extraction as the first step. Three kinds of features will be considered: (1) relative entropy measurement; (2) average energy measurement; (3) normalized center PSD measurement. We will discuss them in detail next subsections.

### 2.5.1 Support Vector Machine (SVM)

SVM is originally applied in a two-class classification problem. For multiple class classifications, it is usually extended to  $n$  class classification by constructing  $n$  two-class classifiers, and then picks the best over all classifiers. The geometrical interpretation of support vector classification (SVC) is that the algorithm searches for the optimal separating surface, i.e. the hyperplane that is, in a sense, equidistant from the two classes. This optimal separating hyperplane has many nice statistical properties. SVC is outlined first for the linearly separable case. Kernel functions are then introduced in order to construct non-linear decision surfaces.

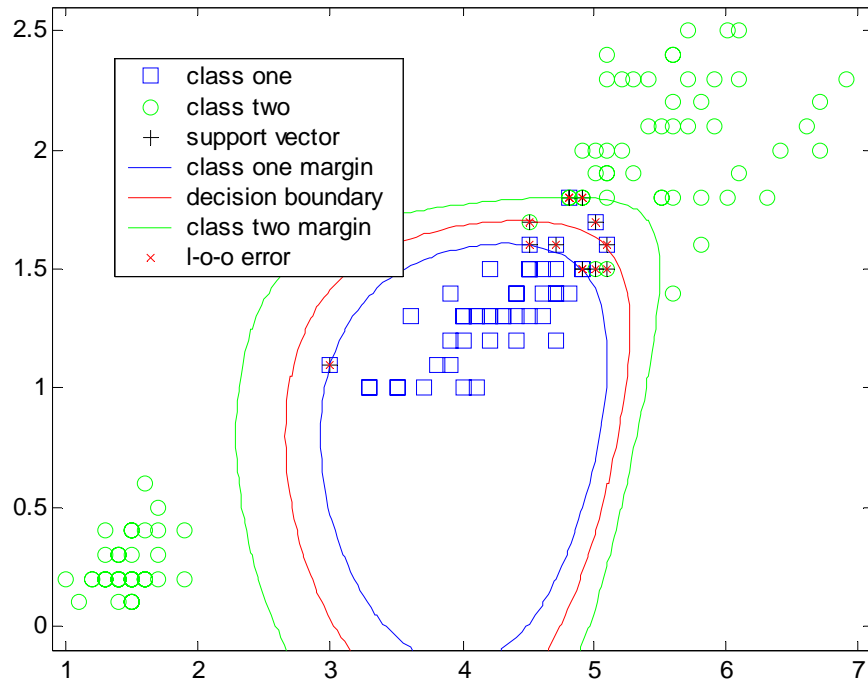


Fig. 18 Example of applying SVM to separate two classes of data

Fig. 18 shows the concept of SVM. The line with “+” is the optimal boundary separating the two classes. Unlike other classifiers, the SVM classifier focuses only on boundary data points, called support vectors. When performing data classification, only support vector information is used to construct the classifier.

A linear classifier may not be the most suitable hypothesis for the two classes. This can be particularly true in target recognition as targets may exhibit highly nonlinear behaviors. The

SVM can be used to learn non-linear decision functions by first mapping the data to some higher dimensional feature space and constructing a separating hyperplane in this space.

A common approach to generate kernels is to define a positive definite kernel that corresponds to a known classifier such as a Gaussian RBF, two-layer MLP or polynomial classifier. This “kernel trick” gives the SVM great flexibility. With a suitable choice of parameters an SVM can separate any consistent data set (that is, one where points of distinct classes are not coincident).

The advantages of SVM include:

- It is a quadratic learning algorithm; hence, there are no local optima. It can also be formed as linear programming for simplicity.
- Statistical theory gives bounds on the expected performance of a support machine.
- Performance is better than most learning systems for a wide range of applications including automatic target recognition, image detection, and document classification
- Although originally designed for 2-class classification, SVMs have been effectively extended to multi-class classification applications.
- There is no over-training problem as compared to conventional learning classifiers such as neural net or fuzzy logic.

## 2.5.2 Feature Extraction

### Relative Entropy Measurement

The relative entropy measurement is termed the *Kullback Leibler* distance (KL-distance) in literature. It is a natural distance function from a “true” probability distribution,  $p$ , to a “target” probability distribution,  $q$ . It can be interpreted as the expected extra message-length per datum due to using a code based on the wrong (target) distribution compared to using a code based on the true distribution.

For discrete (not necessarily finite) probability distributions,  $p=\{p_1, \dots, p_n\}$  and  $q=\{q_1, \dots, q_n\}$ , the KL-distance is defined to be

$$KL(p, q) = \sum_i p_i \cdot \log_2(p_i / q_i)$$

For continuous probability densities, the sum is replaced by an integral.

$$\begin{aligned} KL(p, p) &= 0 \\ KL(p, q) &\geq 0 \end{aligned}$$

Note that the KL-distance is not, in general, symmetric.

To apply the KL-distance as a feature in our problem, we need first define the “true” and “target” probability distributions. We propose to use absolute correlation values to build the distributions. The case “true” denotes the normal condition (training data), and the case “target” denotes any

condition under testing. For instance, we have waveforms  $x(i,t)$ ,  $i=1,2,\dots$ , the cross correlation is defined as

$$y(i,t) = \text{corr}[x(i,t), x(i-1,t)]$$

The probability distribution is then,

$$\text{Pr}[y(i,t)] = |y(i,t)| / \sum_t |y(i,t)|$$

Using this formula in the training data set and the testing data set, we can easily get the “true” and “target” probability distributions. Specifically, we build the probability distributions  $p$  via the waveform at normal condition training data, and the probability distributions  $q$  via any waveform to be tested.

After normalization processing, the normalized KL-distance measurements are plotted in Fig.19-23 for the five data sets (data11c, data12c, data13c, data14c and data15c, suffix c means post-processed data). Where, the “cup/saucer” locations are denoted with diamond and triangle, respectively. Obviously, this feature discriminates cup/saucer dents in a consistent manor, which is good for classifications.

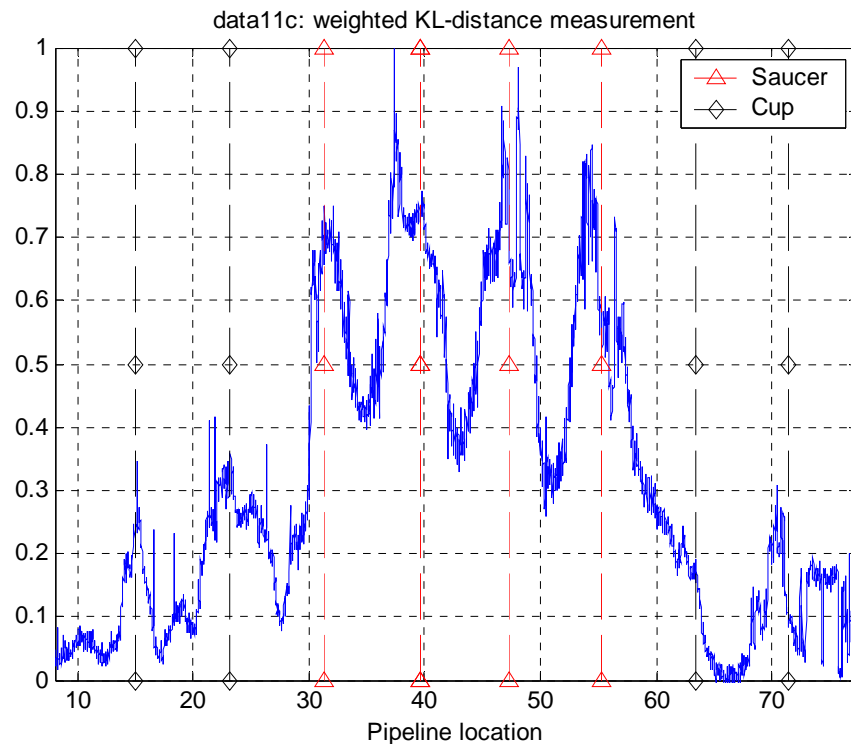


Fig.19 Normalized KL-distance measurement for data11c.

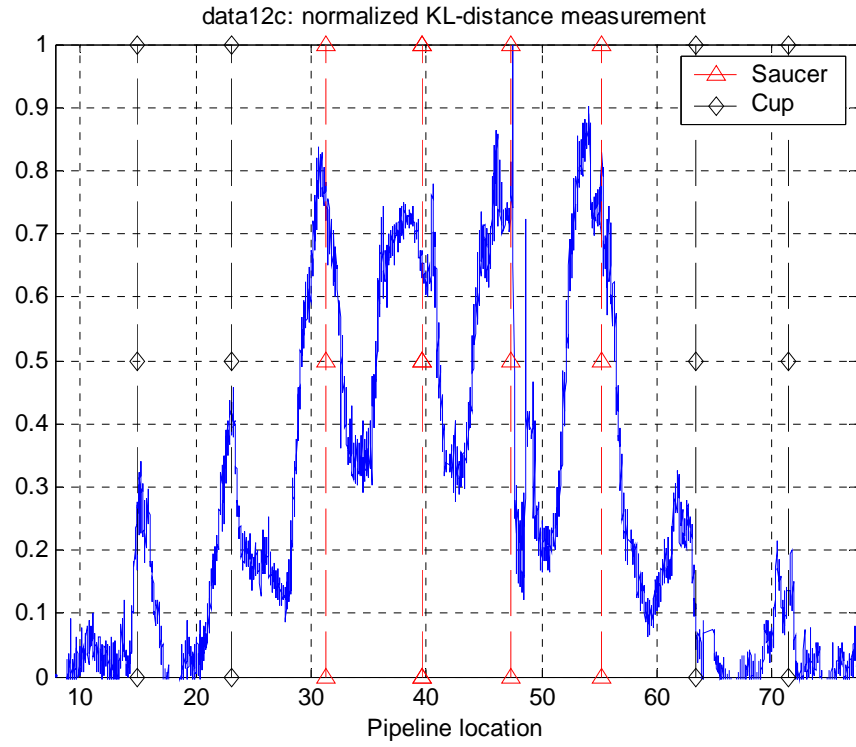


Fig.20 Normalized KL-distance measurement for data12c.

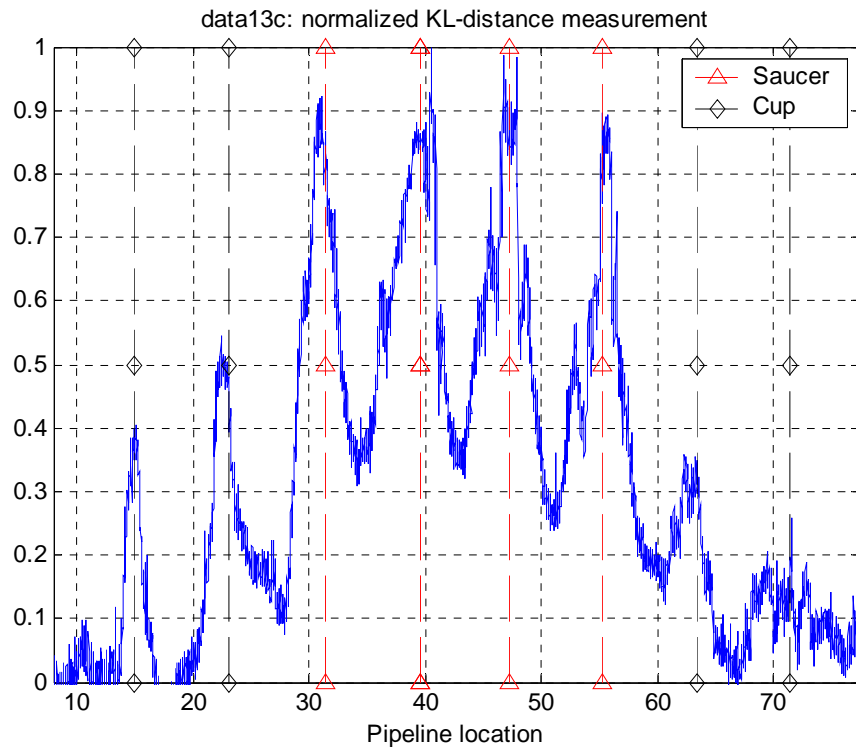


Fig.21 Normalized KL-distance measurement for data13c.

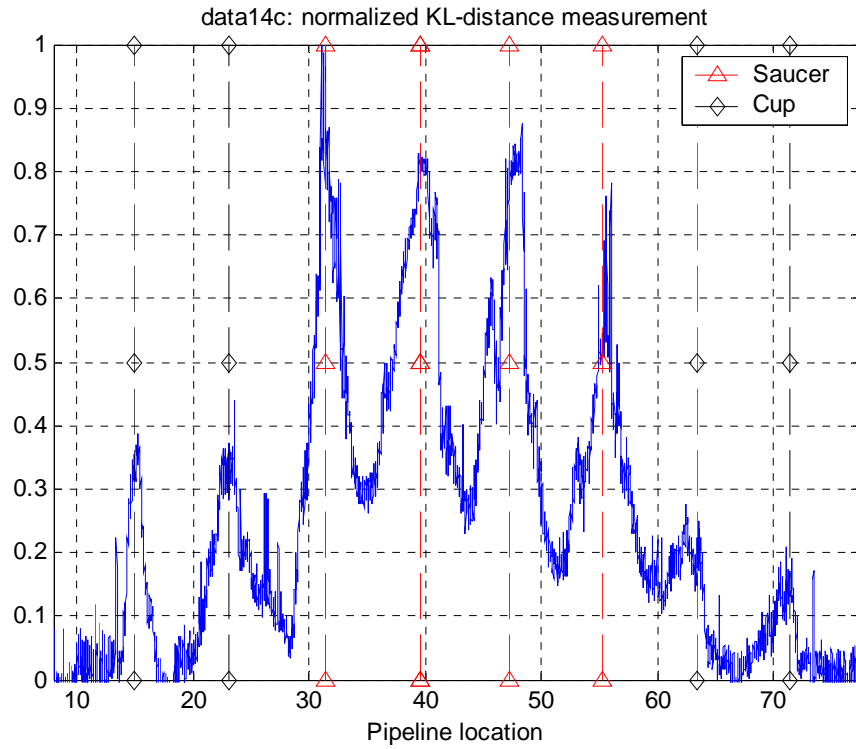


Fig.22 Normalized KL-distance measurement for data14c.

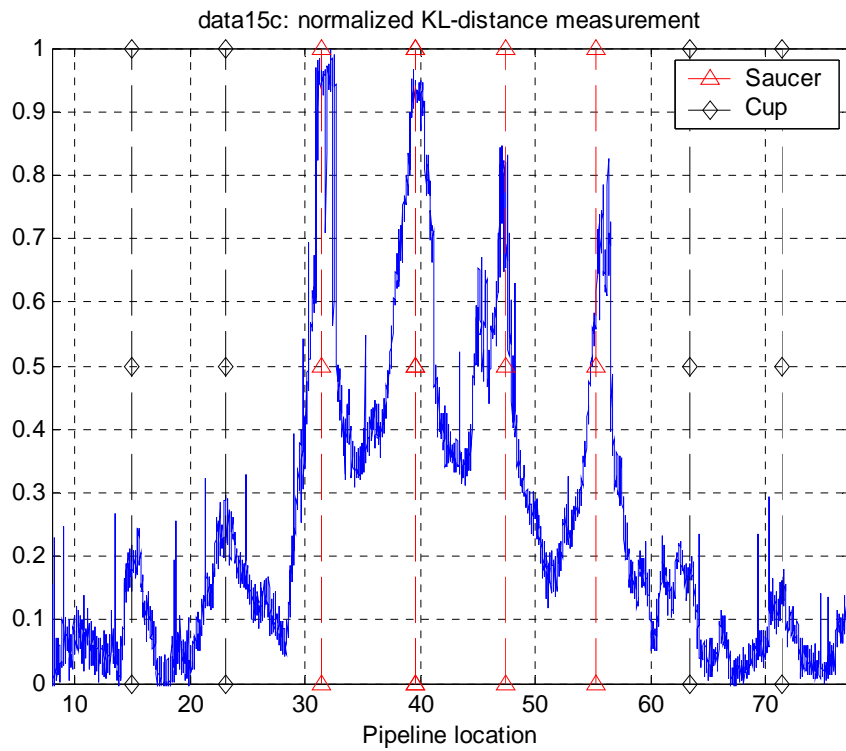


Fig.23 Normalized KL-distance measurement for data15c.

### Average Energy Measurement

Since cup/saucer dents absorb/deflect EMAT waveforms, the energy of the testing waveform will be impacted. This can be a good indication for classification in time domain. For instance, we have waveforms  $x(i,t)$ ,  $i=1,2,\dots$ , the average energy measurement is defined as

$$z(i) = \sum_t x(i,t)*x(i,t)/\text{sample\_size}$$

The average energy measurements are plotted in Fig.24-28 for the five data sets (data11c, data12c, data13c, data14c and data15c).

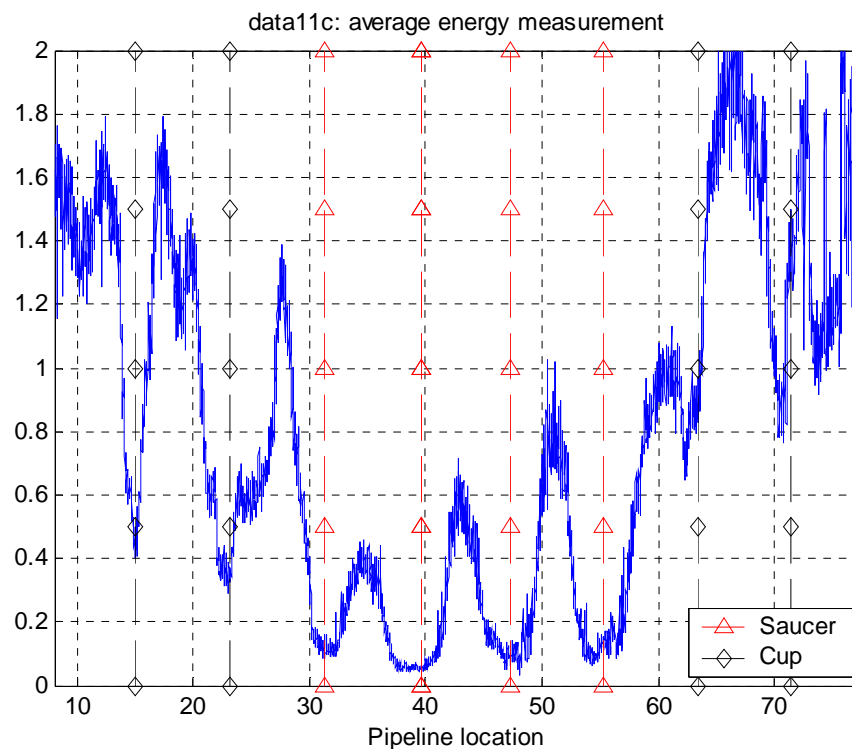


Fig.24 Average energy measurement for data11c.

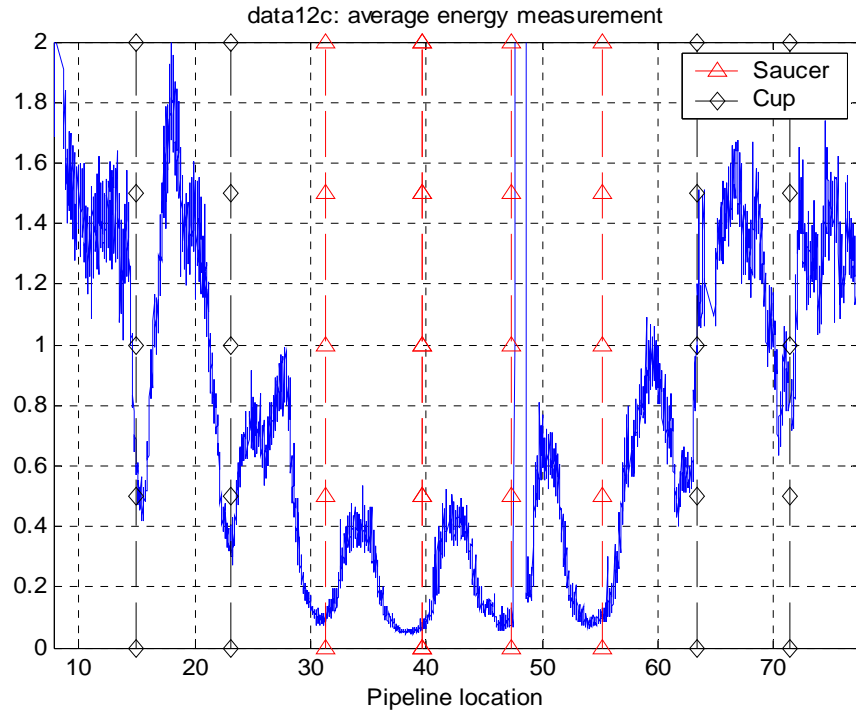


Fig.25 Average energy measurement for data12c.

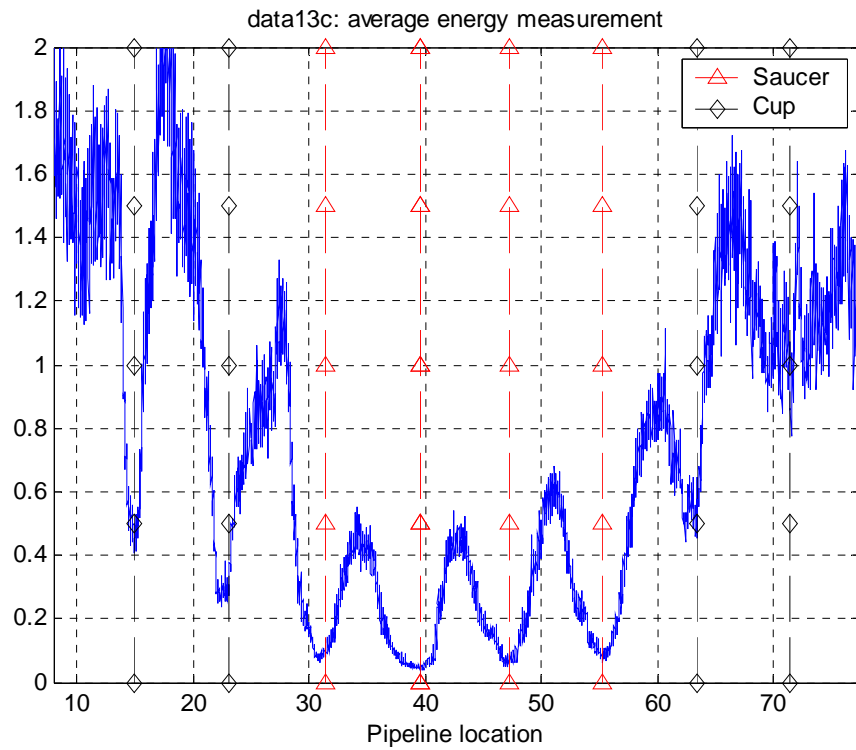


Fig.26 Average energy measurement for data13c.

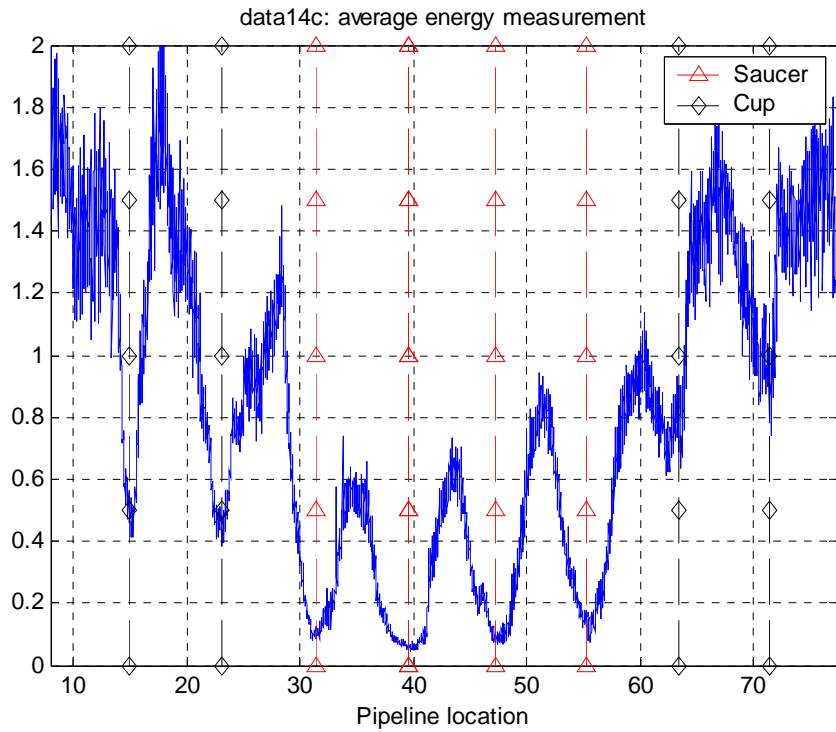


Fig.27 Average energy measurement for data14c.

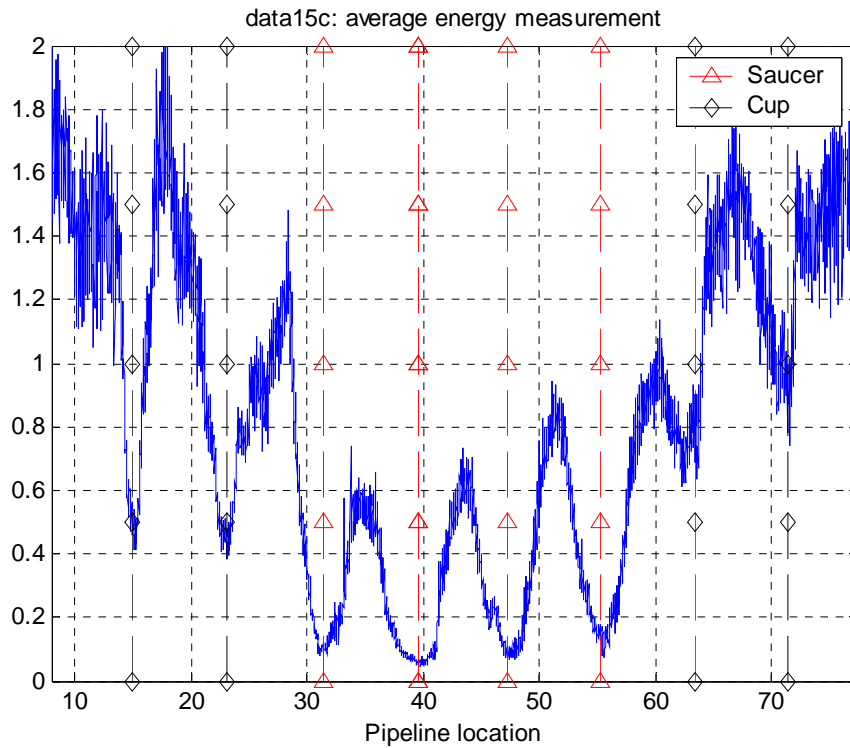


Fig.28 Average energy measurement for data15c.

### Normalized Center PSD Measurement

On the other hand, the spectrum of the EMAT waveform will also be affected due to any damage in pipeline. Usually, there is a center frequency when we generate the EMAT signals for pipeline inspections. Although all the spectrum of the EMAT waveform may provide more information to help classification, there is a computation complexity issue when considering the whole spectrum. However, the center PSD value provides the most important information to indicate the waveform distortions. Therefore, we use normalized center PSD measurement as a feature in the frequency domain. Here the normalization processing is actually a ratio concept, in which the center PSD value in any test condition is divided by that in the normal condition. As an example, Fig.29 demonstrates the center PSD values as the EMAT waveform in normal or dent conditions.

The normalized center PSD measurements are plotted in Fig.30-34 for the five data sets (data11c, data12c, data13c, data14c and data15c).

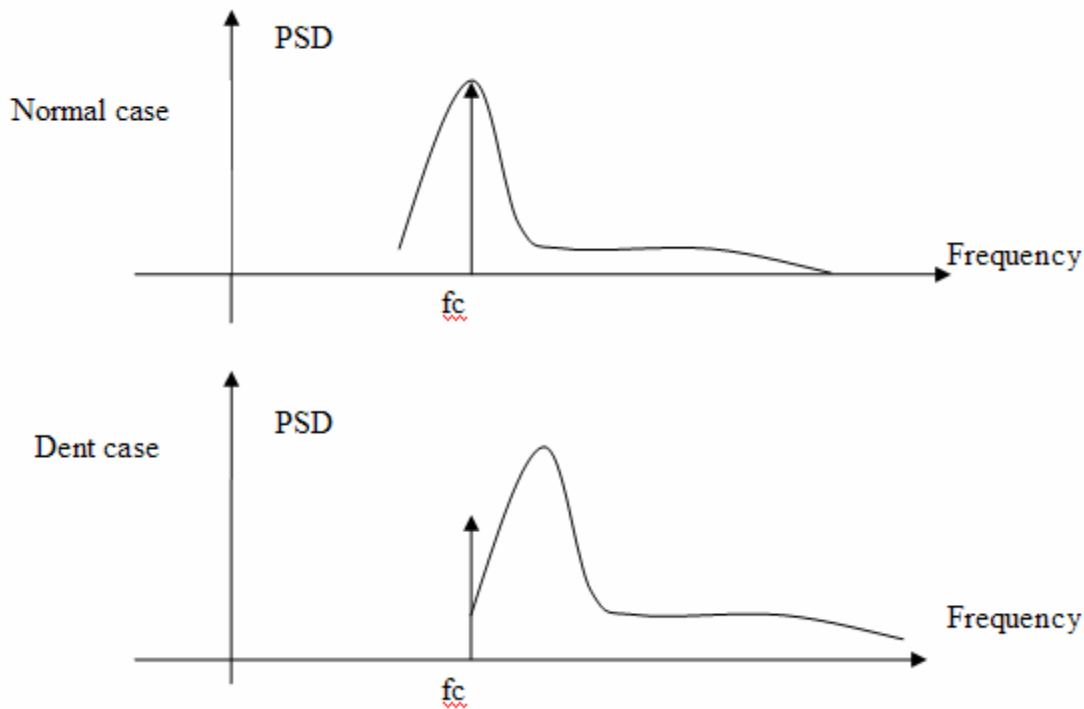


Fig.29 illustration of the center power spectrum density shift as the result of dent

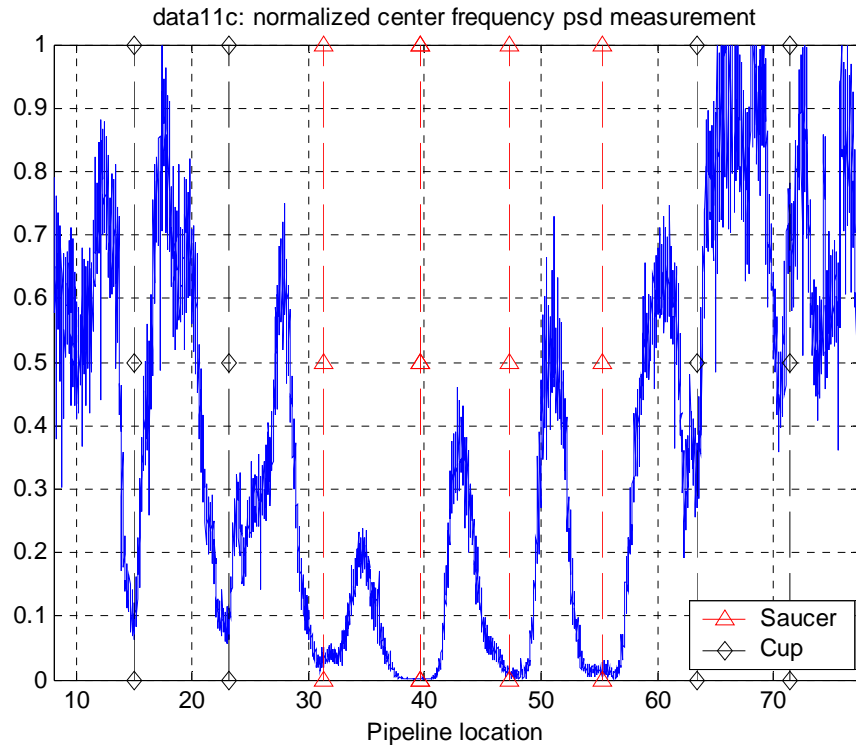


Fig.30 Normalized center frequency PSD measurement for data11c.

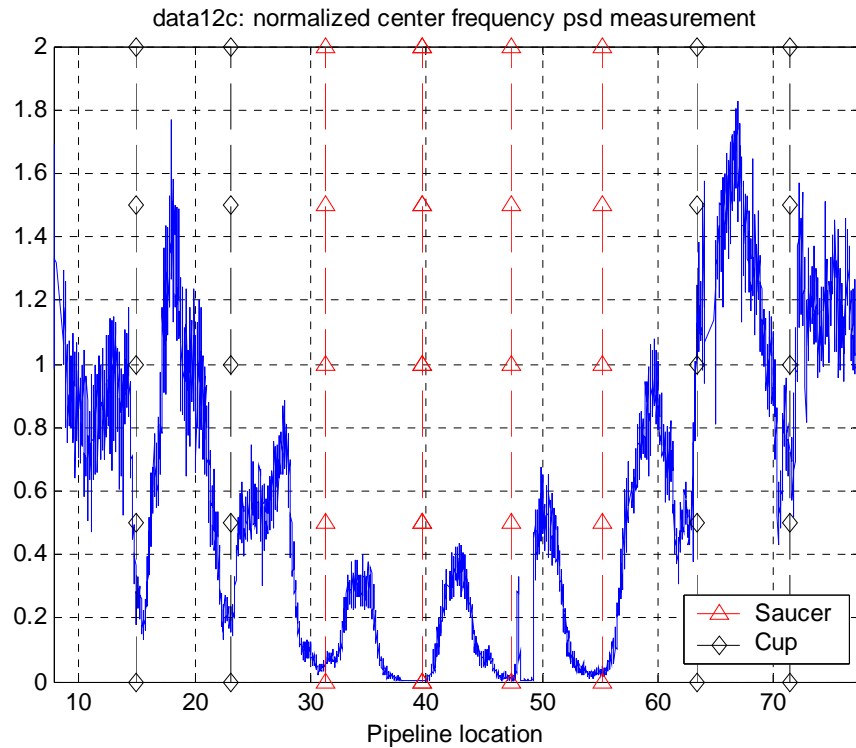


Fig.31 Normalized center frequency PSD measurement for data12c.

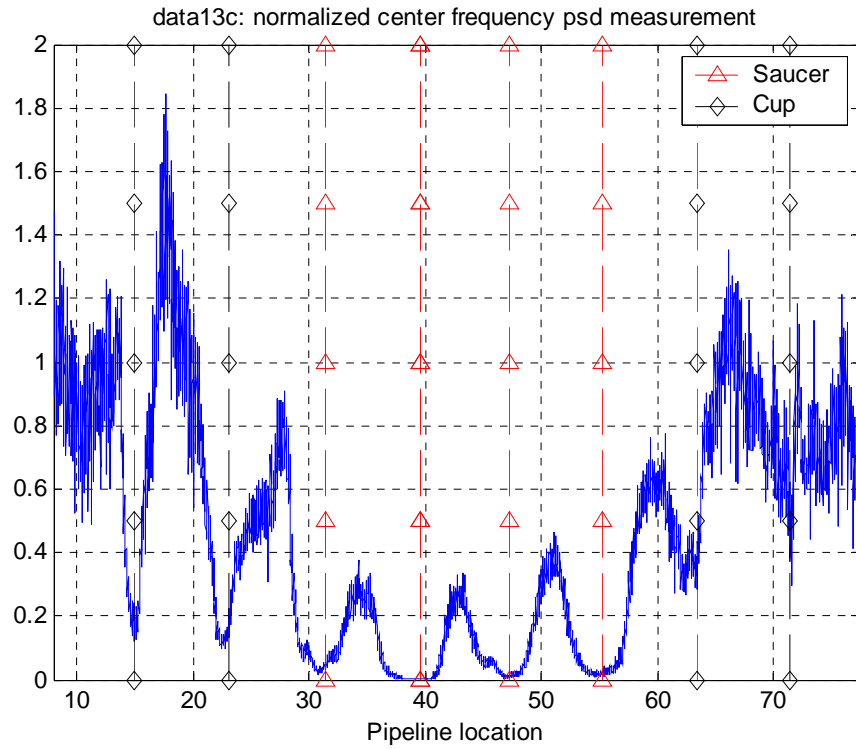


Fig.32 Normalized center frequency PSD measurement for data13c.

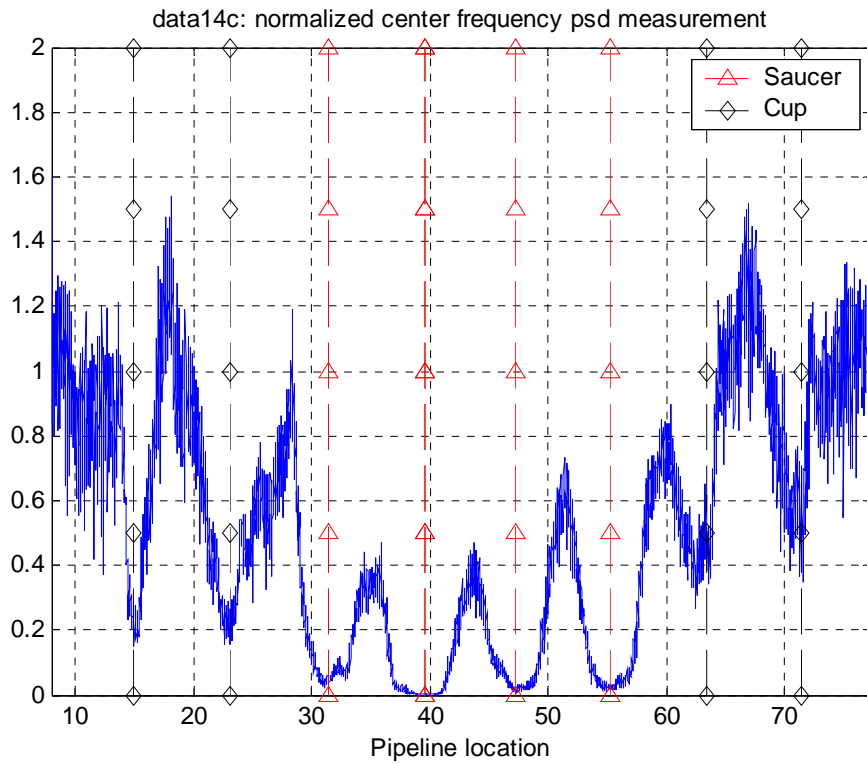


Fig.33 Normalized center frequency PSD measurement for data14c.

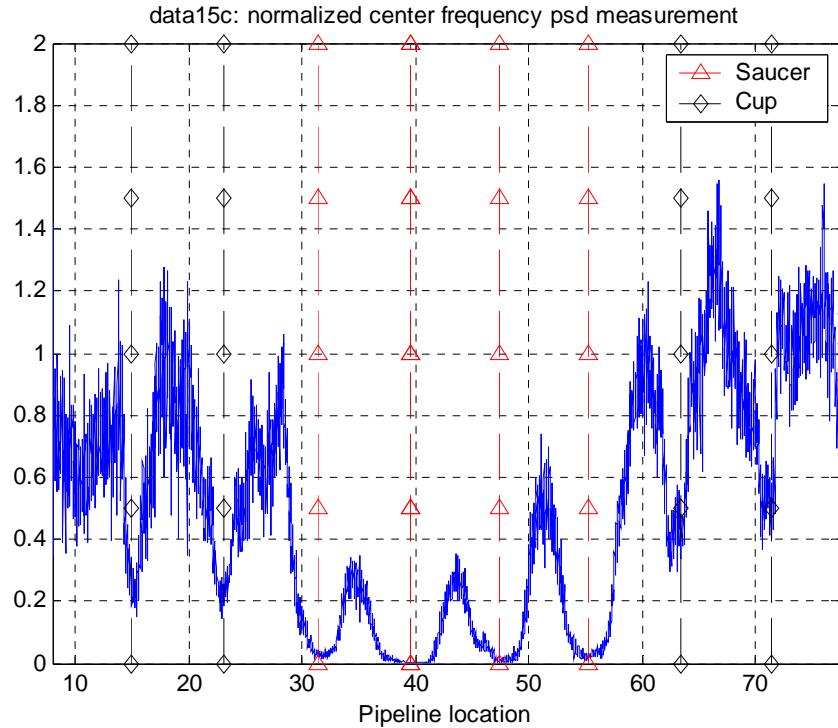


Fig.34 Normalized center frequency PSD measurement for data15c.

### 2.5.3 Performance Evaluations

The five data sets (data11c, data12c, data13c, data14c and data15c) are based on a same experiment setup. Table 1 presents the basic information about the cup/saucer, including size, depth, area of deformation, and so on. The centers of the cup/saucer dents are listed below (the unit is in inch)

Based on the dent information, we define five classes such that

- “1”: normal condition
- “2”: cup deformed region excluding cup dent
- “3”: cup dent
- “4”: saucer deformed region excluding saucer dent
- “5”: saucer dent

In practice, we can combine “2”, “3” to one class of cup dent, and “4”, “5” to one class of saucer to simplify the classification problem. Fig.35-39 plot the five class distributions.

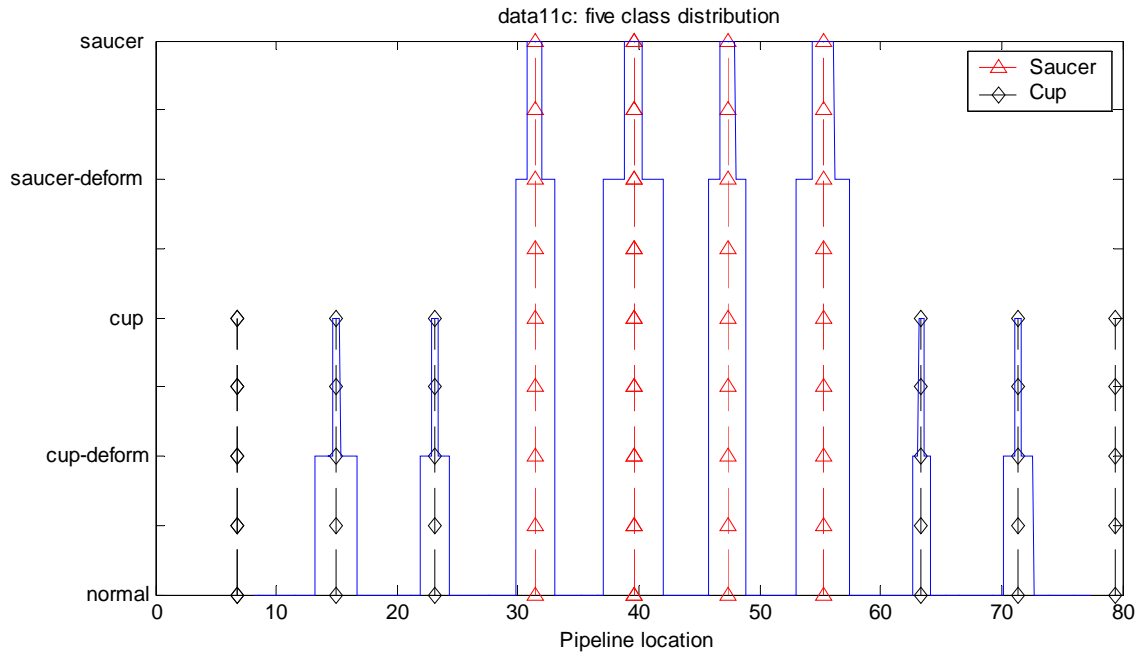


Fig.35 Five class distribution setup for data11c.

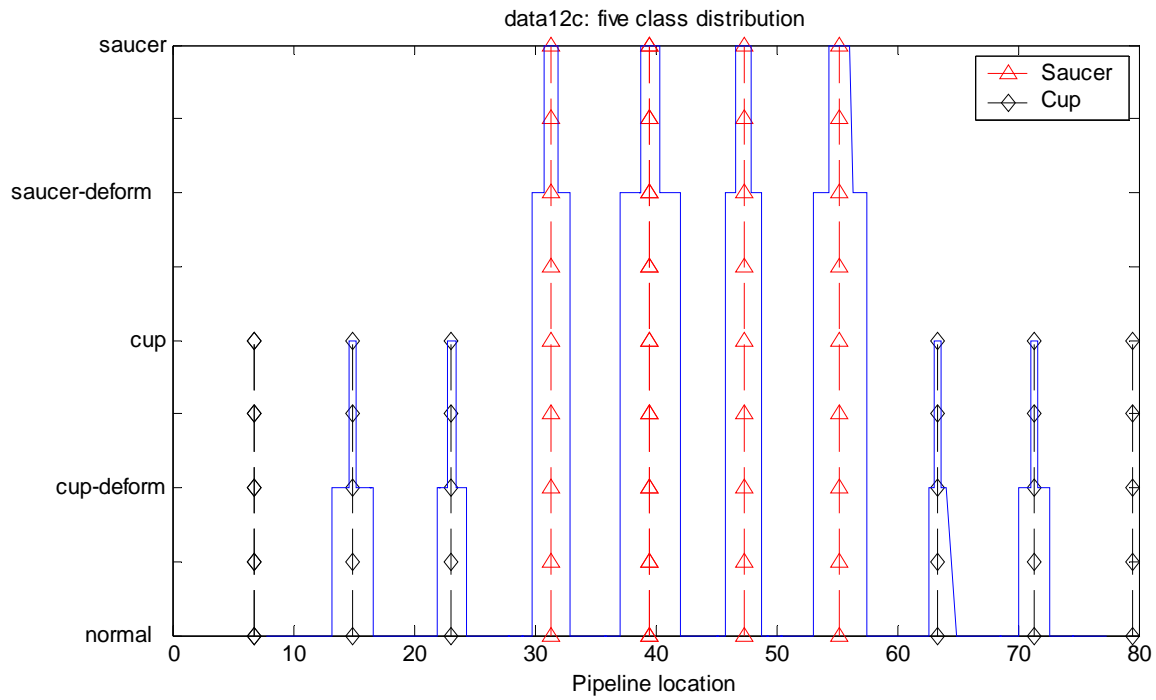


Fig.36 Five class distribution setup for data12c.

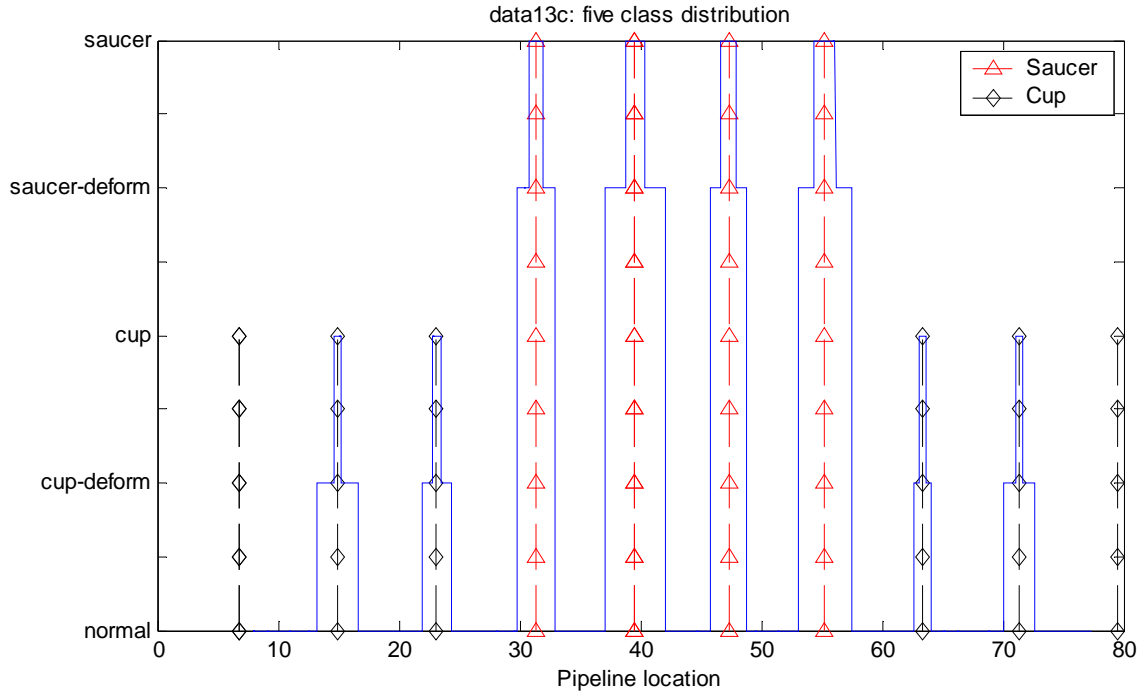


Fig.37 Five class distribution setup for data13c.

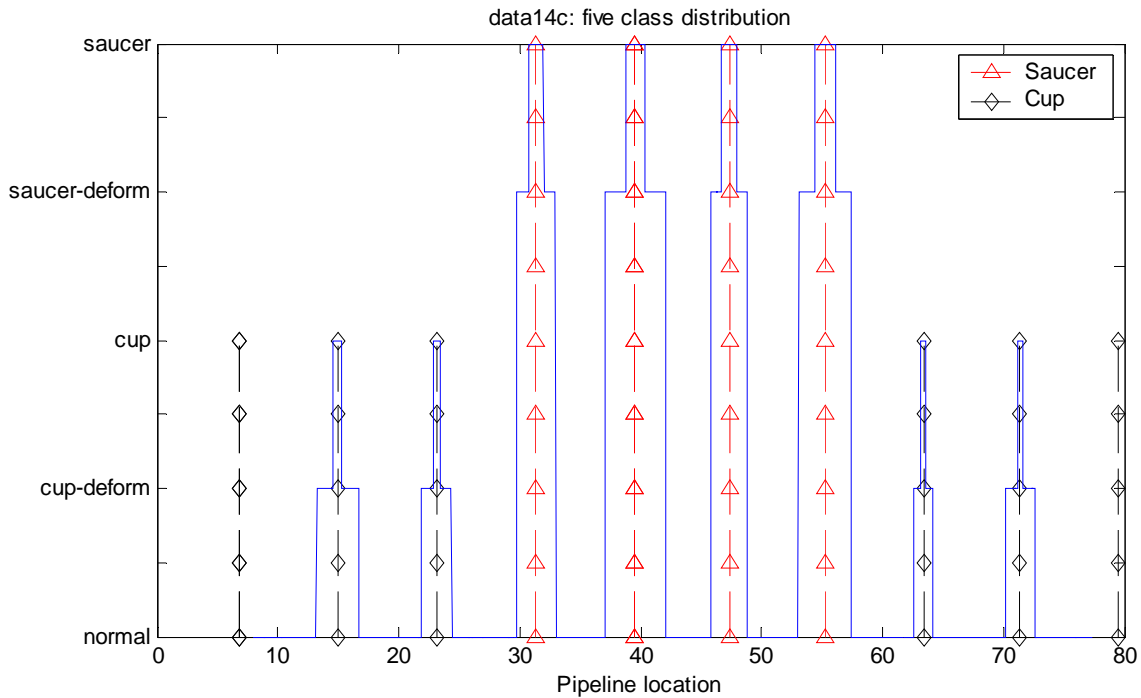


Fig.38 Five class distribution setup for data14c.

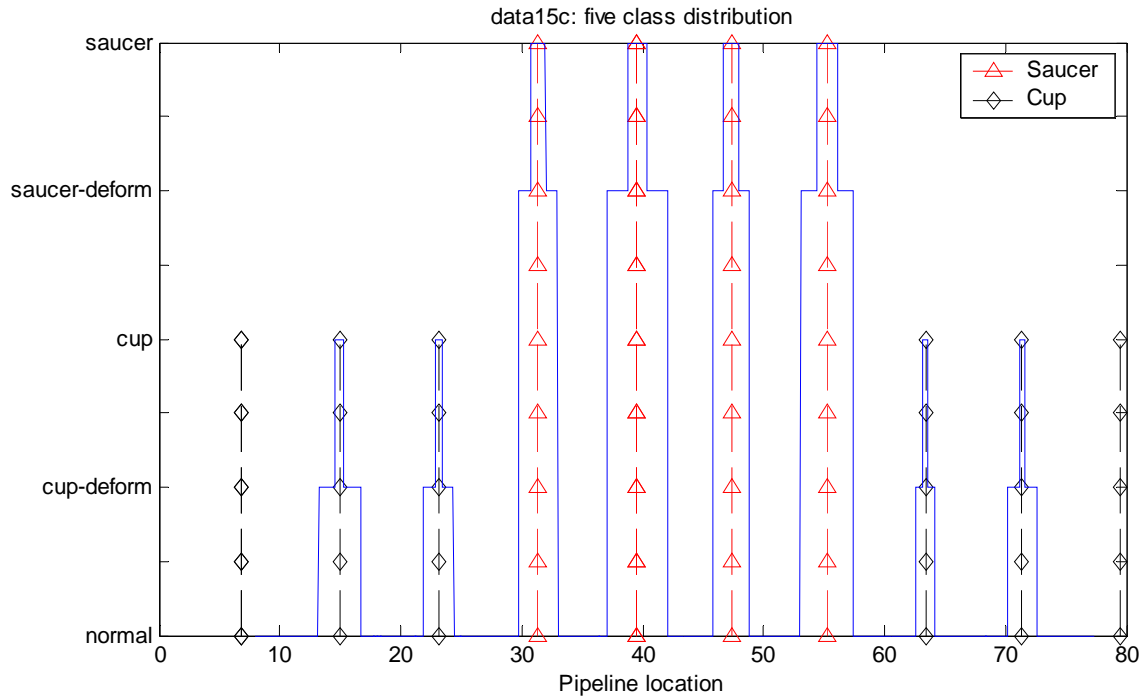


Fig.39 Five class distribution setup for data15c.

**Leave-one-out classification test**

**Scenario I:**

In this scenario, we purely use one data file as training data, and the rest data files as testing data. To train SVM, we use any one data file out of the five data files separately, and then we test other data sets. The results are listed in Table 3.

**Table 3 Classification results when the whole data set of data13c is used as training set**

	Data11c	Data12c	Data13c	Data14c	Data15c
Data11c as training set	--	75.01%	76.29%	76.02%	77.18%
Data12c as training set	74.15%	--	76.26%	74.37%	74.47%
Data13c as training set	76.07%	73.85%	--	82.46%	80.78%
Data14c as training set	75.75%	72.90%	80.75%	--	80.60%
Data15c as training set	76.25%	72.37%	80.76%	82.68%	--

Obviously, the classification performance is about at the range of 72%~83%. The mainly reason is that the conditions among “Saucer” are actually not the normal conditions. However, we treat them still as normal conditions in the evaluations considered. On the other hand, we have used 5 classes to be identified. Between class-“2” and “3”, as well as class-“4” and “5”, the classification results will be impacted a lot. In the next simulation scenario, we will combine “2”, “3” as one class, and “4”, “5” as another class for performance evaluations.

**Scenario II:**

After combining dent-region, and deformed-region as one class, there are only three different classes for identification: (1) normal condition; (2) “Cup” condition; (3) “Saucer” condition. In this evaluation scenario, we combine all five data sets, and build nine groups of data based on the location information. One of them is for the normal condition, and the other eight groups are for 2-Cup, 3-Cup, 4-Saucer, 5-Saucer, 6-Saucer, 7-Saucer, 8-Cup and 9-Cup, respectively. In each group of data sets, we sequentially pick about 500 waveforms. By leaving any one group of data, we first train the SVM classifier using all the left data, and then we test the leaved data. We can also test the trained data for performance comparisons.

**Table 4 SVM Classification Results**

		Leave-one-out training/testing (each item below is leaved out separately)							
		2-Cup	3-Cup	4-Saucer	5-Saucer	6-Saucer	7-Saucer	8-Cup	9-Cup
Dent region	trained data	95.12	95.32	95.36	95.36	95.29	95.30	96.59	98.89
	leaved data	100	82.76	100	100	100	91.99	79.45	65.99

Table 4 illustrates the classification results. The case of “dent region” means that data are obtained from the dent-region area only at cup/saucer conditions. As denoted in the table, each column presents “Leave-one-out” test separately. For instance, considering the column of “2-Cup”, the training data set consists of eight groups of data (exclude the group of data “2-Cup”). “trained\_data” presents the to-be-tested data which is as the same as the training data set, however, “leaved\_data” presents the to-be-tested data which is just the leave-one-out data (the group of data “2-Cup”).

**Comparison test with PCA-DA**

For comparison purpose, we tested the PCA-DA approach that was developed in our previous project. Here we use the 100 waveforms around the detected dent position for our classification purpose. The classification result is shown in the following table.

**Table 5 Dent classification in pipe #1 with PCA-DA**

Results for the data set data11 regarding the Cup/Saucer classification.

	Number of samples	Labeled as Cup	Labeled as Saucer	Accuracy
Cup	16	14	2	88%
Saucer	16	0	16	100%

Results for the data set data12 regarding the Cup/Saucer classification.

	Number of samples	Labeled as Cup	Labeled as Saucer	Accuracy
Cup	16	13	3	81%
Saucer	16	4	12	75%

Results for the data set data13 regarding the Cup/Saucer classification.

	Number of samples	Labeled as Cup	Labeled as Saucer	Accuracy
Cup	16	16	0	100%
Saucer	16	4	12	75%

Results for the data set data14 regarding the Cup/Saucer classification.

	Number of samples	Labeled as Cup	Labeled as Saucer	Accuracy
Cup	16	16	0	100%
Saucer	16	4	12	75%

Results for the data set data15 regarding the Cup/Saucer classification.

	Number of samples	Labeled as Cup	Labeled as Saucer	Accuracy
Cup	16	14	2	88%
Saucer	16	2	14	88%

It is seen that the support vector machine based approach achieves generally better result than our previous PCA-DA approach.

#### 2.5.4 Concluding Remarks

SVM has been introduced as a new approach to classify cup/saucer dents in pipeline with the help of SH wave EMAT signals, from which three features are identified and extracted. The three features are based on the KL-distance, the average energy (time domain) and the center frequency PSD ratio (frequency domain).

Classification performances are mainly evaluated by using the leave-one-out simulation scenario.

Further work will be conducted to evaluate the newly proposed SVM classifier for cup/saucer dents in large different data sets with many different conditions.

### 3. Future Work

We propose to perform the following technical tasks in Phase 2:

- Task 1: Further developments in theoretical studies.
  - Task 1.1: Arrange a kickoff meeting; further refine the pipeline inspection problem and objective.
  - Task 1.2: Further study the guided wave scattering phenomenon from a 3-D perspective so that the detection and classification algorithms have a stronger physics based foundation. Numerical modeling of dents in a pipe with respect to different size, shape, depth, etc. and also different incident frequencies for sensor design and feature extraction.

- Task 1.3: Incorporate coating effect in the numeric modeling, validate the results with experiments
- Task 2: Perform experiments on real pipes with or without coatings
    - In phase I we focused our effort on the feasibility study of our proposed approach for the pipe dents inspection. The pipe specimens were 12-inch diameter. In phase II, we will extend our techniques to both the transmission line and distribution network.
    - Task 2.1: Obtain pipes with or without coatings, produce mechanical dents or other defects on the specimen
    - Task 2.2: Custom design guided SH wave EMAT sensors for the specific pipes, take consideration of the wall thickness change and curvatures.
    - Task 2.3: Perform data collection and validate our detection and classification algorithms.
  - Task 3: Develop mobile platform or integrate our EMAT sensors with existing mobile platforms for either the small diameter pipe or large diameter pipe.
    - Task 3.1: Based on the market needs and DOT engineer input, initiate the design for a mobile fixture for either the gas transmission line or distribution network.
    - Task 3.2: Address the potential problem of pipe curvature change or ovalation, consider mating with CMU platform or existing PIGs
  - Task 4: Further improve and optimize the algorithms developed in Phase 1
    - Task 4.1: Further improve the dents classification rates.
    - Task 4.2: Capability of dent size estimation
    - Task 4.1: Capability to deal with noise
    - Task 4.2: Capability to extract defect signature and deal with new type of defect other than dents
  - Task 5: Implement the algorithms in real-time hardware
    - Task 5.1: Integrate and test the software together in the MATLAB environment
    - Task 5.2: Implement the selected algorithm in the prototype system
    - Task 5.3: Setup the communications between software and hardware; develop the Graphical User Interface (GUI) for the operator
  - Task 6: Perform real-time laboratory tests
    - Task 6.1: Debug the EMAT fixture system hardware and software, perform the real-time test in the pipe specimen.
    - Task 6.2: Evaluate the integrated system
  - Task 7: Perform real-time demonstrations at Oak Ridge National Lab and DOT
    - Task 7.1: Finalize the hardware and software of the prototype EMAT sensor system, package the system for the lab test.
    - Task 7.2: Demonstration of the EMAT system for real-time mechanical dents and possible other defect detection, classification and size estimation

- Task 8: Commercialization
  - Task 8.1: Advertise and demonstrations of the system for industries and other government agencies and industries; attract investments for phase 3 product development.

## **Acknowledgments**

This work is financially supported by U. S. Department of Transportation, PHMSA under contract number DTRT57-06-C-10004. The authors would also like to thank Mr. James Merritt for his supervision of this project.